*Astronomy & Astrophysics* manuscript no. LFI˙Programme˙Paper˙M1˙4may09
May 6, 2009


# The Planck-LFI Programme

N. Mandolesi, M. Bersanelli, C. Burigana, R.C. Butler, G. De Zotti, F. Finelli, A. Gruppuso, S. Matarrese, A. Mennella, G. Morgante, P. Natoli, F. Pasian, M. Sandri, L. Terenzi, F. Villa, A. Zacchei, E. Artal, C. Baccigalupi, A. Banday, K. Bennett, P. Bhandari, A. Bonaldi, M. Bremer, B. Cappellini, T. Courvoisier, G. Crone, F. Cuttaia, L. Danese, O. DArcangelo, R. Davies, R. Davis, L. De Angelis, G.C. De Gasperis, T. Ensslin, M.C. Falvella, M. Frailis, E. Franceschi, T. Gaier, S. Galeotta, F. Gasparo, J. Gonzalez-Nuevo, K. Górski, A. Gregorio, R. Hell, D. Herranz, J.M. Herreros, W. Hovest, R. Hoyland, M. Janssen, E. Keihanen, H. Kurki-Suonio, A. Lahteenmaki, C.R. Lawrence, S. Leach, P. Leahy, R. Leonardi, S. Levin, P.B. Lilje, S. Lowe, P.M. Lubin, D. Maino, M. Malaspina, M. Maris, J. Marti-Canales, E. Martinez-Gonzalez, F.T. Matthai, P. Meinhold, L. Mendes, G. Morigi, N. Morrisset, A. Nash, R. Nesti, C. Paine, B. Partridge, D. Pearson, L. Peres-Cuevas, F. Perrotta, L.A. Popa, T. Poutanen, M. Prina, J. Rachen, R. Rebolo, M. Reinecke, S. Ricciardi, T. Riller, G. Rocha, N. Roddis, J.A. Rubino, D. Scott, M. Seiffert, J. Silk, A. Simonetto, G.F. Smoot, C. Sozzi, J. Sternberg, L. Stringhetti, J. Tauber, M. Tomasi, J. Tuovinen, M. Türler, D. Uwe, L. Valenziano, J. Varis, P. Vielva, N. Vittorio, L. Wade, S. White, A. Wilkinson, A. Zonca

[1] IASF - BO, INAF, Bologna, Italy
[2] Dipartimento di Fisica, Università degli Studi di Milano,Italy
[3] Osservatorio Astronomico di Padova, INAF, Italy
[4] Dipartimento di Fisica, Univeristà degli Studi di Padova, Italy
[5] Dipartimento di Fisica, Univeristà degli Studi di Roma "Tor Vergata", Italy
[6] Osservatorio Astronomico di Trieste, INAF, Italy
[7] SISSA, Trieste, Italy
[8] ISDC, University of Geneva, Versoix, Switzerland
[9] Dipartimento di Fisica, Universita' degli Studi di Trieste,Italy
[10] Jodrell Bank Observatory, Jodrell Bank, U.K.
[11] Physics Department, University of California at Santa Barbara, USA
[12] ESA - ESAC (Madrid), Spain
[13] Istituto di Fisica del Plasma, CNR, Milano, Italy
[14] Instituto de Fisica De Cantabria, Consejo Superior de Investigaciones Cientificas, Universidad de Cantabria, Spain
[15] .....

Preprint online version: May 6, 2009

**Abstract**

*Context.* This paper provides an overview of the Low Frequency Instrument (LFI) programme within the ESA Planck mission.
*Aims.* The LFI instrument has been developed to produce high precision maps of the microwave sky at frequencies in the 27÷77 GHz range, below the peak of the Cosmic Microwave Background (CMB) radiation spectrum.
*Methods.* The scientific goals are described, ranging from mainstream cosmology to Galactic and extragalactic astrophysics. The instrument design and development is outlined, together with the model philosophy and testing strategy. The instrument is presented in the context of the Planck mission. The LFI approach to on-ground and in-flight calibration is described. We also provide a description of the LFI ground segment. We present results of a number of tests that demonstrate the capability of the LFI Data Processing Centre (DPC) to properly reduce and analyse LFI flight data, from telemetry information to sky maps and other scientific products. The organization of the LFI Consortium is briefly presented as well as the role of the Core Team.
*Results.* All tests carried out on the LFI flight model show the excellent performance of the various sub-units and of the instrument as a whole. The data analysis pipeline has been tested and its main functionalities proved.
*Conclusions.* The commissioning, calibration, performance, and verification phases will be performed during the first three months after launch. After this, Planck will start its operational life, which LFI appears ready to support.

**Key words.** (Cosmology): Cosmic Microwave Background – Galactic and extragalactic astrophysics – Space vehicles – Calibration – Data analysis

## 1. Introduction

In 1992 the Cosmic Background Explorer (COBE) team announced the discovery of intrinsic temperature fluctuations in the cosmic microwave background (CMB) on angular scales larger than 7° at a level of a few tens of $\mu$K Smoot et al. (1992a). One year later two space-borne CMB experiments were proposed to the European Space Agency (ESA) in the framework of the Horizon 2000 Scientific Programme: the Cosmic Background Radiation Anisotropy Satellite (COBRAS), an array of receivers based on High Electron Mobility Transistor (HEMT) amplifiers, and the SAtellite for Measurement of Background Anisotropies

The address to which the proofs have to be sent is:
Nazzareno Mandolesi
INAF-IASF Bologna, Via Gobetti 101, I-40129, Bologna, Italy
fax: +39-051-6398681
e-mail: mandolesi@iasfbo.inaf.it

(SAMBA), an array of detectors based on bolometers. The two proposals were accepted for assessment study with the recommendation to merge. In 1996 ESA selected a combined mission called COBRAS/SAMBA, subsequently renamed Planck, as the third Horizon 2000 Medium-Sized Mission. Today Planck forms part of "Cosmic Vision 2020" ESA Programme.

Planck is equipped with a 1.5 m effective aperture telescope which will scan the sky in nine frequency channels from 30 GHz to 857 GHz with its two active cooled instruments, the Low Frequency Instrument (LFI) operating at 20 K with pseudo-correlation radiometers and the High Frequency Instrument (HFI) whose bolometers operate at 100 mK. LFI and HFI together will have a sensitivity up to 10 times better and angular resolution up to 3 times better than the Wilkinson Microwave Anisotropy Probe (WMAP). The use of two different instrument technologies and the comparison between their data will allow an optimal control and suppression of systematic effects. All the LFI channels and four of the HFI channels are sensitive to linear polarisation.

Today Planck, the first European and third generation mission after COBE and WMAP, is the best CMB anisotropy probe in space. The Planck payload (telescope, instruments and cooling chain) is indeed a single, highly integrated space-borne CMB experiment. While HFI is more sensitive and achieves slightly better angular resolution, it is only the combination of the two instruments that will achieve the tight control of systematic and astrophysical effects necessary for the full exploitation of Planck data. However, each of the two instruments has its own specific role in the programme. The present paper describes the principal scientific goals of LFI, its instrument characteristics and programme.

Planck retains the heritage from the original proposal COBRAS in the optical concept, an aplanatic Gregorian off axis telescope with a wide focal plane containing the two instruments.

LFI consists of an array of 11 corrugated horns feeding 22 polarisation sensitive pseudo-correlation radiometers based on HEMT transistors and MMIC technology which are actively cooled down to 20 K by a new concept sorption cooler specifically designed to deliver high efficiency, long duration cooling power. The radiometers cover three frequency bands centred at 30 GHz, 44 GHz, and 70 GHz. The design of the radiometers has been driven by the need to minimize the introduction of systematic errors and suppress noise fluctuations generated in the amplifiers.

The design of the horns is optimized for achieving beams with the highest resolution in the sky together with the lowest side lobes. Typical LFI main beams have full width half maximum (FWHM) resolutions of about 33′, 27′, and 13′, respectively at 30 GHz, 44 GHz, and 70 GHz. The beams are approximately elliptical with ellipticity ratio (i.e. major/minor axis) of $\simeq 1.15 \div 1.40$. The beam profiles will be measured in flight by observing planets and strong radio sources (Burigana et al. 2001).

A summary of the LFI performance requirements adopted to drive the instrument design is reported in Table 1.

The requirement to minimize systematic effects has imposed stringent constraints also on the thermal behaviour, at the point that the Planck cryogenic architecture is one of the most complicated ever conceived for space. Moreover, the spacecraft has been designed to exploit the favorable thermal conditions of the L2 orbit. The thermal system is a combination of passive and active cooling: passive radiators are used as thermal shields and pre-cooling stages, while active cryocoolers are used both for instruments cooling and pre-cooling. The cryochain consists of the following main sub-systems (Collaudin & Passvogel 1999):

- pre-cooling from 300 K to about 50 K by means of passive radiators in three stages (≈150 K, ≈100 K, ≈50 K), which are called V-Grooves due to their conical shape;
- cooling to 18 K for LFI and pre-cooling the HFI 4 K cooler via a $H_2$ Joule-Thomson Cooler with sorption compressors (the Sorption Cooler);
- cooling to 4 K for pre-cooling the HFI dilution refrigerator and for the LFI reference loads via a Helium Joule-Thomson cooler with mechanical compressors;
- cooling of the HFI to 1.6 K and finally 0.1 K with an open loop $^4$He-$^3$He dilution refrigerator.

The LFI front end unit is maintained at its operating temperature by the Planck $H_2$ Sorption Cooler Sub-system (SCS): a closed-cycle vibration-free continuous cryocooler designed to provide 1.2 Watt of cooling power at a temperature of 18 K. Cooling is achieved by hydrogen compression, expansion through a Joule-Thomson valve and liquid evaporation at the cold stage. The Planck SCS is the first long-duration system of its kind to be flown on a space platform. Operations and performances are described in more detail in Sect. 3.3 and in Morgante (2009b).

Planck is a spinning satellite. Thus, its receivers will observe the sky through a sequence of (almost great) circles following a scanning strategy (SS) aimed at minimizing systematic effects and achieving all-sky coverage for all receivers. Several parameters are relevant for the SS. The main one is the angle, $\alpha$, between the spacecraft spin axis and the telescope optical axis. Given the extension of the focal plane unit, each beam centre points to its specific angle, $\alpha_r$. The angle $\alpha$ is set to 85° to achieve a nearly all-sky coverage even in the so-called *nominal* SS in which the spacecraft spin axis is kept always exactly along the antisolar direction. This choice avoids the "degenerate" case $\alpha_r = 90°$, characterized by a concentration of the crossings of scan circles only at the ecliptic poles and then the degradation of the quality of destriping and map making codes (Burigana et al. 1999; Maino et al. 1999a). Since the Planck mission is designed to minimize the straylight contamination by Sun, Earth, and Moon (Burigana et al. 2001; **?**), it is possible to introduce modulations of the spin axis from the ecliptic plane to maximize the sky coverage keeping constant the solar aspect angle of the spacecraft for thermal stability. This drives towards the adopted *baseline*

**Table 1.** LFI performance requirements. The average sensitivity per 30' pixel or per FWHM$^2$ resolution element ($\delta$T and $\delta$T/T, respectively) is given here in CMB temperature (i.e. equivalent thermodynamic temperature) for 14 months of integration. The white noise per frequency channel and 1 sec of integration in given in antenna temperature.

| Frequency channel | 30GHz | 44GHz | 70GHz |
|---|---|---|---|
| InP detector technology | MIC | MIC | MMIC |
| Angular resolution [arcmin] | 33 | 24 | 14 |
| $\delta$T per 30' pixel [$\mu$K] | 8 | 8 | 8 |
| $\delta$T/T per pixel [$\mu$K/K] | 2.67 | 3.67 | 6.29 |
| Number of radiometers (or feeds) | 4 (2) | 6 (3) | 12 (6) |
| Effective bandwidth [GHz] | 6 | 8.8 | 14 |
| System noise temperature [K] | 10.7 | 16.6 | 29.2 |
| White noise per $\nu$ channel [$\mu$K $\cdot \sqrt{s}$] | 116 | 113 | 105 |
| Systematic effects [$\mu$K] | $< 3$ | $< 3$ | $< 3$ |

http://wmap.gsfc.nasa.gov

SS (Maris et al. 2006). Thus, the baseline SS adopts a cycloidal modulation of the spin axis, i.e. a precession around a nominal antisolar direction with a semiamplitude cone of 7.5°. In such a way all Planck receivers will cover the whole sky. A cycloidal modulation with a 6 month period satisfies the mission operational constraints while avoiding sharp gradients in the pixel hit count (Dupac & Tauber 2005). Furthermore, this solution allows to spread the crossings of scan circles in a wide region which is beneficial to map making, particularly for polarization (Ashdown et al. 2007b). The last three SS parameters are: the sense of precession (clockwise or anticlockwise), the initial spin axis phase along the precession cone, and, finally, the spacing between two consecutive spin axis repointings, chosen at 2′ to achieve four all-sky surveys with the available guaranteed number of spin axis manoeuvres.

LFI is the result of an active collaboration among about a hundred universities and research centres, in Europe, Canada and USA, organized in the LFI Consortium (supported by more than 300 scientists) funded by national research and space agencies. The Principal Investigator leads a team of 26 Co-Investigators responsible for the development of the instrument hardware and software. The hardware has been developed under the supervision of an Instrument Team. The data analysis and its scientific exploitation is mostly carried out by a Core Team of about 100 scientists, working in close connection with the Data Processing Centre (DPC). The Core Team is closely linked to a Planck wider scientific community, comprising, other than LFI, the HFI and Telescope Consortia, organized in a structure of Working Groups. Planck is managed by the ESA Planck Science Team.

The paper is organized as follows. In Section 2 we report the LFI scientific objectives and role in the mission. Section 3 is devoted to the LFI optics, radiometers and Sorption Cooler set up and performances. The LFI programme is set forth in Section 4. LFI Data Processing Center is illustrated in Section 6 after a a report of the LFI tests and verifications in Section 5. Conclusions are drawn in Section 7.

## 2. Cosmology and astrophysics with LFI

Planck is the third generation space mission for CMB anisotropies and will open a new era in the understanding of the Universe. Planck will measure cosmological parameters with a much greater level of accuracy than all previous efforts. Furthermore, its high resolution all-sky survey, the first ever in the microwave range, will feed the astrophysical community for years to come.

### *2.1. Cosmology*

The LFI 70 GHz channel is located within a frequency window remarkably clear from foreground emissions and thus particularly advantageous to observe the CMB, in both temperature and polarization. Thus, the LFI instrument will play a crucial role for cosmology.

The two lowest LFI frequency channels working at 30 GHz and 44 GHz provide an accurate monitor of Galactic and extra-Galactic foreground (see Sect. 2.2) whose removal (see Sect. 2.3) is critical for the success of the Planck mission. This aspect is of particular relevance for polarization since Galactic emission dominates the polarized sky.

#### 2.1.1. Large scale anomalies

Observations of anisotropies of cosmic microwave backgroung (CMB) radiation contributed to the building of the standard cosmological model, also known as concordance model, involving a set of parameters on which CMB observations and other cosmological and astrophysical data sets agree: spatial curvature close to zero, almost 70% of dark energy, 20÷25% of cold dark matter (CDM), 4÷5% of baryonic matter, nearly scale invariant adiabatic Gaussian primordial perturbations. Although the data coming from the anisotropy pattern of CMB obtained by WMAP are largely consistent with the concordance ΛCDM model, there are some interesting and curious deviations from it, in particular on the largest angular scales. They have been obtained with detailed analyses and can be listed as follows. *1) Lack of power at large scales*. The angular correlation function is found to be uncorreleted (i.e. consistent with 0) for angles larger than 60°. In (Copi et al. 2008, 2007) it has been shown that this event happens 0.03% of realizations of the concordance model. Still in this category we mention the surprisingly low amplitude of the quadrupole term of the angular power spectrum (APS), already found by COBE (Smoot et al. 1992b; Hinshaw et al. 1996), and now confirmed by WMAP (Dunkley et al. 2009; Komatsu et al. 2009). *2) Unlikely alignments of low multipoles*. An unlikely (for a statistically isotropic random field) alignment of the quadrupole and the octupole is described in reference (Tegmark et al. 2003; Copi et al. 2004; Schwarz et al. 2004; Weeks 2004; Land & Magueijo 2005). Moreover, both quadrupole and octupole align with the CMB dipole Copi et al. (2007). Other unlikely alignments are described in Abramo et al. (2006). *3) Hemispherical asymmetries*. It is found that the power coming separately from the two hemispheres (defined by the ecliptic plane) is too asymmetric (especially at low $\ell$) (Eriksen et al. 2004a,b). *4) Cold Spot*. Vielva et al. (2004) detected a non Gaussian behaviour in the southern hemisphere with a wavelet analysis technique.

It is still unknown if these anomalies can be considered as hints of new (and fundamental) physics beyond the concordance model or if they are the residual of some not perfectly removed astrophysical foreground or systematic effect. Planck data will give a precious contribution not only to refine the cosmological parameters of the standard cosmological model but also to solve the aforementioned puzzles thanks to a better foreground removal and control of systematic effects. In particular, the LFI 70 GHz channel will be crucial to this scientific aim, since, as probed by WMAP, the foreground at large angular scales in minimum in the V band.

#### 2.1.2. Sensitivity to CMB angular power spectra

The statistical information enclosed in CMB anisotropies, in both temperature and polarization, can be analyzed in terms of a “compressed” estimator, the angular power spectrum (APS) which, provided that anisotropies obey Gaussian statistics, as predicted in a wide class of models, contains most of the relevant statistical properties. The quality of the recovered APS is a good tracer of the efficiency in extracting cosmological parameters through a comparison with theoretical predictions arising from Boltzmann codes. Strictly speaking, the latter task must be carried out through likelihood analyses. Neglecting systematic ef-

The above nominal SS is kept as backup solution in the case of a possible verification in flight of an unexpected, bad behaviour of Planck optics.

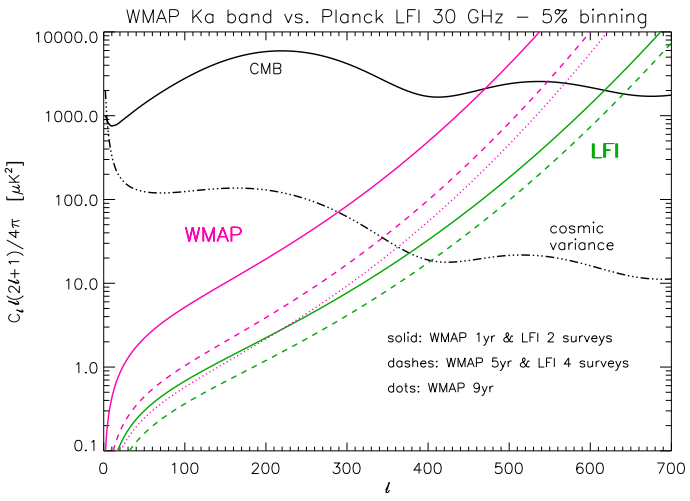


**Figure 1.** CMB temperature anisotropy APS (black solid line) compatible with WMAP data are compared to WMAP (Ka band) and LFI (30 GHz) sensitivity to the APS (Knox et al. 1995), assuming subtracted the noise expectation, for different integration times as reported in the figure.The plot report separately the cosmic variance (black three dot-dashes) and the instrumental noise (red and green lines for WMAP and LFI, respectively) assuming a multipole binning of 5%. Regarding sampling variance, an all-sky survey is assumed here for simplicity.

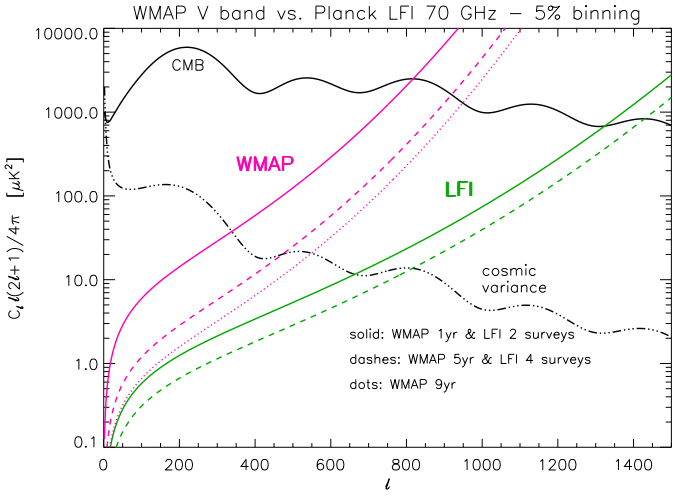


**Figure 2.** As in Fig. 1 but for the sensitivity of WMAP in V band and LFI at 70 GHz.

fects (and correlated noise), the sensitivity of a CMB anisotropy experiment to APS, $C_\ell$, at each multipole $\ell$ is summarized by the equation (**?**)

$$\frac{\delta C_\ell}{C_\ell} \simeq \sqrt{\frac{2}{f_{\rm sky}(2\ell+1)}}\left[1+\frac{A\sigma^2}{NC_\ell W_\ell}\right], \qquad (1)$$

where $A$ is the size of the surveyed area, $f_{\rm sky} = A/4\pi$, $\sigma$ is the rms noise per pixel, $N$ is the total number of observed pixel, and $W_\ell$ is the beam window function. For a symmetric Gaussian beam $W_\ell = \exp(-\ell(\ell+1)\sigma_{\rm B}^2)$ where $\sigma_{\rm B} = {\rm FWHM}/\sqrt{8\ln 2}$ defines the beam resolution.

Even in the limit of an experiment with infinite sensitivity ($\sigma = 0$) the accuracy on the APS is limited by the so-called cosmic and sampling variance, reducing to pure cosmic variance in the case of all-sky coverage ($f_{\rm sky} = 1$), which is quite relevant at

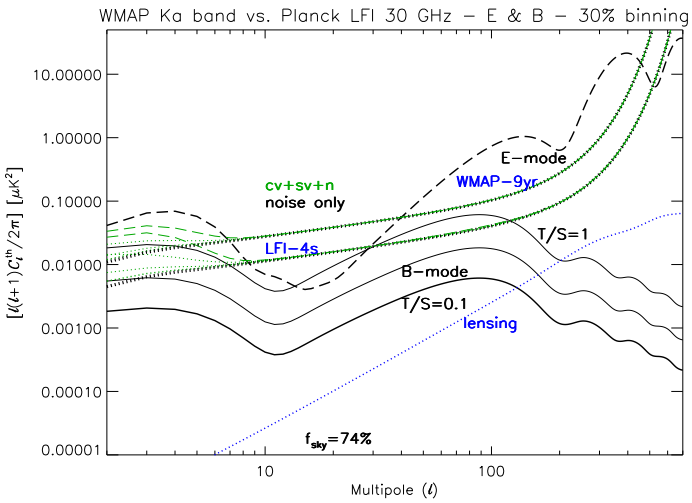


**Figure 3.** CMB E polarization modes (black long dashes) compatible with WMAP data and CMB B polarization modes (black solid lines)for different tensor-to-scalar ratios of primordial perturbations ($T/S = 1, 0.3, 0.1$, at increasing thickness) are compared to WMAP (Ka band, 9 years of observations) and LFI (30 GHz, 4 surveys) sensitivity to the APS (Knox et al. 1995), assuming subtracted the noise expectation. The plots include cosmic and sampling variance plus instrumental noise (green dots for B modes, green long dashes for E modes, labeled with cv+sv+n; black thick dots, noise only) assuming a multipole binning of 30%. Note that the cosmic and sampling (74% sky coverage) variance implies a dependence of the overall sensitivity at low multipoles on $T/S$ (again the green lines refer to $T/S = 1, 0.3, 0.1$, from top to bottom), which is relevant for parameter estimation; instrumental noise only determines capability to detect the B mode. The B mode induced by lensing (blue dots) is shown for comparison.

low $\ell$ because of the relatively small number of available modes $m$ per multipole in the spherical harmonic expansion of sky map. The multifrequency maps that will be obtained with Planck will allow to improve the foreground subtraction and to maximize the effective sky area used in the APS analysis, thus improving with respect to previous experiments in the knowledge of the low multipole region of CMB APS.

At intermediate and high multipoles, the Planck sensitivity and resolution will produce a significant step forward over previous CMB anisotropy experiments. Clearly, given the telescope size, the angular resolution naturally increases with frequency. Also, foreground fluctuations are frequency dependent. Therefore, an appropriate comparison between the performance of different projects should consider the most similar frequency bands.

Figs. 1 and 2 compare WMAP and LFI sensitivity to CMB APS of temperature anisotropy at two similar frequency bands displaying separately the uncertainty coming from cosmic variance and instrumental performance and considering different project lifetimes. For an easier comparison, we consider the same multipole binning (in both cosmic variance and instrumental sensitivity). The figures show how the multipole region where cosmic variance dominates over instrumental sensitivity moves to higher multipoles in the case of LFI and that the LFI 70 GHZ channel allows to extract information on about two additional acoustic peaks with respect to those achievable with the corresponding WMAP V band.

In this comparison, we exploit the LFI realistic optical and instrumental performances as described in the following sections.

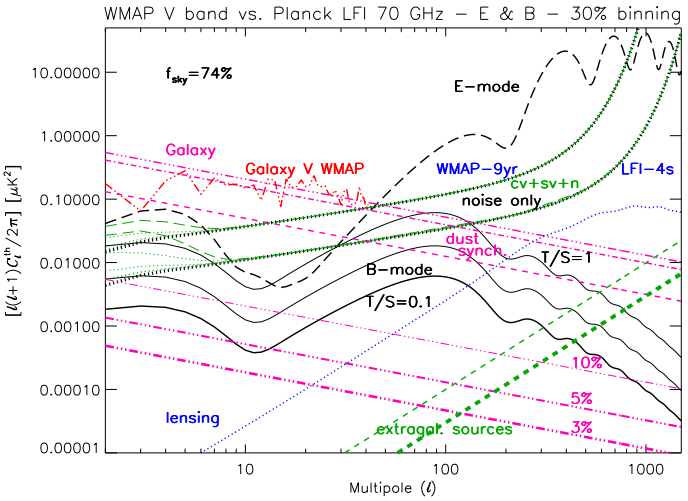


**Figure 4.** As in Fig. 3 but for the sensitivity of WMAP in Ka band and LFI at 70 GHz, and including also the comparison with Galactic and extragalactic polarized foregrounds. Galactic synchrotron (purple dashes) and dust (purple dot-dashes) polarized emissions produce the overall Galactic foreground (purple three dot-dashes). WMAP 3-yr power-law fits for uncorrelated dust and synchrotron have been used. For comparison, WMAP 3-yr results derived directly from the foreground maps are shown on a suitable multipole range: power-law fits provide (generous) upper limits for the power at low multipoles. (For simplicity, we report here only the WMAP results found for the Galactic B mode, that are different from those found for the E mode, but much less remarkably than for the case of CMB modes). Residual contaminations by Galactic foregrounds (purple three dot-dashes) are shown for 10%, 5%, and 3% of the map level, at increasing thickness, as labeled in the figure. The residual contribution by unsubtracted extragalactic sources, $C_\ell^{\rm res,PS}$ and the corresponding uncertainty, $\delta C_\ell^{\rm res,PS}$ computed assuming a relative uncertainty $\delta\Pi/\Pi = \delta S_{\rm lim}/S_{\rm lim} = 10\%$ in the knowledge of their degree of polarization and in the determination of the source detection threshold, are also plotted as green dashes, thin and thick, respectively.

A similar comparison is shown in Figs. 3 and 4 but for the E and B polarization modes considering in this case only the longest mission lifetimes (9 yrs for WMAP, 4 surveys for Planck) reported in previous figures and a larger multipole binning: note the increasing of signal-to-noise ratio. Clearly, foregrounds are much more critical in polarization than in temperature. At the WMAP V band and the LFI 70 GHz channels the polarized foreground is minimum (at least considering a very large sky fraction and up to the range of multipoles already explored by WMAP). Thus, we consider these optimal frequencies to show the potential uncertainty expected from polarized foregrounds. While the Galactic foreground dominates over the CMB B mode and also over the CMB E mode up to multipoles of several tens, a foreground subtraction at 5÷10% accuracy at map level is enough to make Galactic residual contamination well below the CMB E mode and below the CMB B mode for a wide range of multipoles. If we will be able to model Galactic polarized foregrounds at several % accuracy, at the LFI 70 GHz channel the main limitation will come from the instrumental noise which will prevent an accurate E mode evaluation at $\ell \sim 7 \div 20$ and the B mode detection at $T/S \lesssim 0.3$. Clearly, a better recovery of the APS polarization modes will come from the exploitation of the Planck at all frequencies and in this context LFI data will be crucial to better model the polarized synchrotron emission which is necessary to remove at some % accuracy (or better) at map level to be able to detect primordial B modes for $T/S \lesssim 0.1$.

### 2.1.3. Cosmological parameters

Given the improvement with respect to WMAP in APS recovery, achievable with the better sensitivity and resolution of Planck (as discussed in the previous section for LFI), a correspondingly better determination of cosmological parameters is expected. Of course, the great HFI sensitivity joined to the frequency location of its channels, higher than those of WMAP and LFI, and their corresponding higher resolution, will largely contribute to the Planck sensitivity.

We present here the comparison between the determination of a suitable set of cosmological parameters with WMAP, Planck, and Planck LFI alone.

In Fig. 5 we report the forecasts of $1\sigma$ and $2\sigma$ contours for 4 cosmological parameters of the WMAP5 best-fit $\tau\Lambda$CDM cosmological model as expected from Planck LFI 70 GHz channel after 14 months of observations (red lines) compared with the Planck combined sensitivity for the 70 GHz, 100 GHz, and 143 GHz channels for the same integration time (blue lines) and WMAP five year observations (black lines). We have taken the 70 GHz channels and the 100 GHz and 143 GHz as the representative channels for LFI and HFI (note that for HFI we have used angular resolution and sensitivities as given in the Planck Scientific Programme **?**) for cosmological purposes, respectively, and considered a coverage of the 85% of the sky.

While we have not explicitly considered the other channels of LFI – 30 GHz and 44 GHz – and HFI – at frequencies $\geq$ 217 GHz – note that their are essential to achieve accurate separation of the CMB from astrophysical emission.

The improvement on cosmological parameters from LFI (2 surveys) with respect to WMAP 5 is clear from Fig. 5 . This is maximized for the dark matter abundance $\Omega_c$ due to the better performance of the LFI 70 GHz channel with respect to WMAP 5. From Fig. 5 it is clear that the improvement which we will get from Planck in the cosmological parameters compared to WMAP 5 can open a new stage in the understanding of cosmology.

### 2.1.4. Primordial non-Gaussianity

Planck data in total intensity and polarization will either provide the first actual meaurement of non-Gaussianity (NG) in the primordial curvature perturbations, or tighten the existing constraints, based on WMAP data, by almost an order of magnitude.

Probing primordial NG is another activity that must be carried out on foreground cleaned maps. Hence, the frequency maps of both instruments must be used to this purpose.

A very important point is that the primordial NG is *model dependent*. As a consequence of the assumed flatness of the inflaton potential any intrinsic NG during standard single-field slow-roll inflation is generally small, hence adiabatic perturbations originated by the quantum fluctuations of the inflaton field during standard inflation are nearly Gaussian distributed. Despite the simplicity of the inflationary paradigm, however, the mechanism by which perturbations are generated is not yet fully established and various alternatives to the standard scenario have been considered. Non-standard scenarios for the generation of primordial perturbations in single-field or multi-field inflation indeed allow for larger NG levels. Moreover, alternative scenarios for the generation of the cosmological perturbations like the

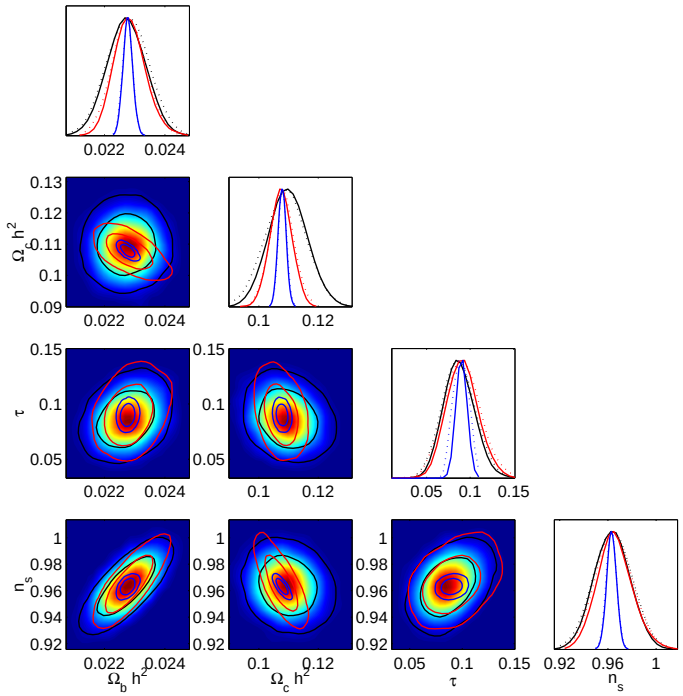


**Figure 5.** Forecasts of $1\sigma$ and $2\sigma$ contours for the cosmological parameters of the WMAP5 best-fit $\tau\Lambda$CDM cosmological model as expected from Planck (blue lines) and from LFI alone (red lines) after 14 months of observations. The black contours are those obtained from WMAP five years observations. See the text for more details.

so-called curvaton, the inhomogeneous reheating and DBI scenarios, are characterized by a potentially large NG level (see, e.g. Bartolo et al. (2004), for a review). For this reason detecting or even just constraining primordial NG signals in the CMB is one of the most promising ways to shed light on the physics of the Early Universe.

The standard way to parametrize primordial non-Gaussianity is as follows. The primordial gravitational potential $\Phi$ is written as

$$\Phi = \Phi_L + f_{\rm NL}\left(\Phi_L^2 - \left\langle\Phi_L^2\right\rangle\right) ,$$

where $\Phi_L$ is a Gaussian random field and $f_{\rm NL}$ is a dimensionless parameter measuring the expected level of quadratic NG. In more generality, the parameter $f_{\rm NL}$ should be replaced by a suitable function, and the product by a (double) convolution. Standard single-field slow-roll inflation produces $f_{NL}$ ($f_{NL} \ll 1$, while much larger values of $|f_{\rm NL}|$ are allowed by the non-standard inflationary models mentioned above.

For this reason both a positive measurement of the non-Gaussianity strength $f_{\rm NL}$ or an upper limit on its amplitude represent a crucial observational discriminant between competing models for the primordial perturbation generation. A positive detection of $f_{\rm NL} \sim 10$ would imply that all standard single-field slow-roll models of inflation are ruled out. On the contrary, an improvement of the limits on the amplitude of $f_{\rm NL}$ will allow to strongly reduce the class of non-standard inflationary models allowed by the data, thus providing a unique clue on the fluctuation generation mechanism. At the same time, Planck data in temperature and polarization will allow to test different predictions for the *shape* of non-Gaussianities. Here, shape of NG essentially refers to the triangle configurations (in harmonic space) yielding the dominant contribution to the angular bispectrum of temperature anisotropies (and polarization). Indeed, it has been shown that the above model, with constant $f_{\rm NL}$ is dominated by so-called "squeezed" triangle configurations, for which one multipole, say $\ell_1$, is much smaller than the other two: $\ell_1 \ll \ell_2, \ell_3$. This "local" NG is typical of models which produce the perturbations right after inflation (such as for the curvaton or the inhomogeneous reheating scenarios). So-called DBI inflation models, based on non-canonical kinetic terms for the *inflaton* (the scalar field which drives inflation), lead to non-local forms of NG, which are dominated by equilateral triangle configurations: $\ell_1 \approx \ell_2 \approx \ell_3$. Recently, it has been pointed out (Holman & Tolley (2008)) that excited initial states for the inflaton may lead to a third shape, called "flattened" triangle configuration. Thus, the shape information provides another important test for the physical mechanism which generated the initial seeds of CMB anisotropies and large-scale structure formation.

The strongest available CMB limits on $f_{\rm NL}$ for local NG comes from WMAP 5-yr data. In particular, Senatore et al. (Smith et al. (2009a)) have obtained $-4 < f_{\rm NL} < 80$ at 95% C.L. using the optimal estimator for local NG. Planck data in total intensity and polarization will allow to reduce the above window on $|f_{\rm NL}|$ below $\sim 10$ (Yadav et al. (2007)). Notice that accurate measurement of E-type polarization will play a relevant role for this result. Note also that the limits that Planck can achieve in this case are very close to those for an "ideal" experiment. Equilateral-shape NG is less strongly constrained at present. The WMAP team (**?**08) obtained $-151 < f_{\rm NL} < 253$ at 95% C.L.. Also in this case, Planck will have a strong impact on this constraint. Indeed, various authors (Smith & Zaldarriaga (2006); Bartolo & Riotto (2009)) have estimated that Planck data will allow us to reduce the bound on $|f_{\rm NL}|$ down to around 70.

Measuring the primordial non-Gaussianity in CMB data to such levels of precision requires accurate handling of possible contaminants, such as those introduced by instrumental noise, mask and imperfect foreground and point source removal. These aspects are presently being dealt with by the Planck team, also with the help of synthetic maps of the CMB including primordial NG as well as realistic models for the various contaminants.

### 2.2. Astrophysics

The accuracy of the extraction of the CMB anisotropy pattern from Planck maps largely relies on the quality of the separation of the *background* signal of cosmological origin from the various *foreground* sources of astrophysical origin that are superimposed into the maps (see also Sect. 2.3). This is particularly critical in polarization where a simple masking of highly contaminated sky regions at low and middle Galactic latitudes is unsatisfactory even for first order analyses. A minimal approach could focus only on the separation of the CMB from all the other components. On the contrary, the Planck scientific programme foresees a full exploitation of the multifrequency data aimed at the separation of each astrophysical component. This will allow to carry out a wealth of astrophysical studies using Planck data alone or in combination with other data sets.

For the sake of brevity, in the next subsections we discuss a few topics relevant for the so-called Planck secondary science and for the LFI Consortium.

More precisely we refer to Bardeen's gauge-invariant gravitational potential, which is such that the CMB anisotropy $\Delta T/T \to -\Phi/3$ in the pure Sachs-Wolfe limit.

### 2.2.1. Galactic Astrophysics

Planck will carry out all-sky survey of the fluctuations of Galactic emissions at its nine frequency bands. At $\nu > 100$ GHz the main improvement with respect to COBE will come from the HFI channels, that will be crucial for the understanding of the Galactic dust emission, still poorly known particularly in polarization.

The LFI frequency channels will be relevant for the study of diffuse synchrotron and free-free Galactic emissions, in particular through the channels at 30 GHz and 44 GHz. While synchrotron emission is significantly polarized, free-free emission is essentially unpolarized. Also, Galactic dust emission still dominates over free-free and synchrotron at 70 GHz, where LFI will provide crucial information on the low frequency tail of this component.

Results from the WMAP lowest frequency channels suggest the presence of a further contribution, likely correlated with dust. While a model in terms of complex synchrotron emission pattern and spectral index cannot be excluded, several interpretations, and in particular the recent ARCADE 2 results, seem to support the identification of this anomalous component in terms of spinning dust.

The improvement in sensitivity and resolution with respect to WMAP achievable with LFI, in particular at 30 GHz, will put new light on this intriguing question. Furthermore, the full interpretation of the Galactic diffuse emissions in Planck maps will benefit from the joint analysis with radio and far-IR data. For instance PILOT will measure polarized dust emission at frequencies higher than 353 GHZ while recent all-sky surveys at 1.4 GHz (**mettere ref**) and in the range few GHz to 15 GHz will complement the low frequency side. A joint analysis of LFI and radio data will be relevant for an accurate understanding of the depolarization phenomena at low and intermediate Galactic latitudes. The detailed knowledge of the underling noise properties in Planck maps will allow one to measure the correlation characteristics of diffuse component greatly improving physical models for the interstellar medium (ISM). The ultimate goal of these studies is the development of a consistent Galactic 3D model, which includes the various components of the ISM and the large and small scale magnetic fields.

While at moderate resolution and limited in flux to a few hundred mJy , Planck will also provide multifrequency, all-sky information on discrete Galactic sources, from stars at early and late stages of their evolution, to HII regions and cold cores. Models for the enrichment of the ISM and for the interplay between stellar formation and ambient physical properties will be further tested.

Planck will have also a chance to observe some bright Galactic sources (like e.g. Cygnus X) in a flare phase and perform a multifrequency monitoring of these events on timescales from hours to weeks.

Finally, Planck will provide a crucial information for the modeling of the emission from Solar System moving objects and diffuse interplanetary dust. The mm and sub-mm emission from planets and up to 100 asteroids will be studied. Moreover the Zodiacal Light Emission will be measured with great accuracy, free from residual Galactic contamination.

At far-IR frequencies significantly higher than those covered by Planck great information comes from IRAS (**?**).

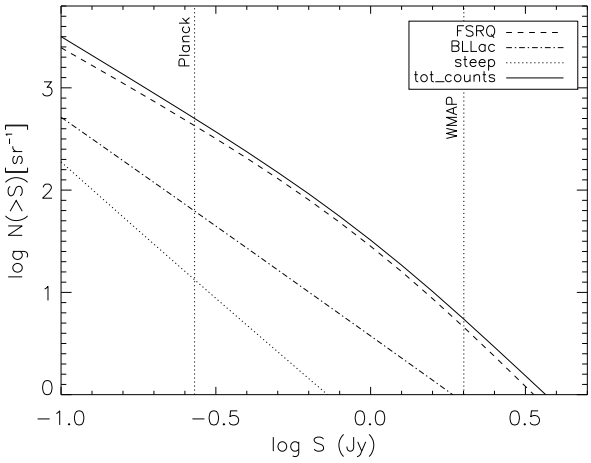


**Figure 6.** Integral counts of different radio source populations at 70 GHz (flat-spectrum radio quasars, FSRQs; BL Lac objects, steep-spectrum sources), as predicted by the De Zotti et al. (2005) model. The vertical dotted lines show the estimated completeness limits for Planck and WMAP (61 GHz) surveys (see text).

### 2.2.2. Extragalactic Astrophysics

WMAP has provided the first all-sky surveys at wavelengths shorter than 5 cm, and the only blind surveys available so far at mm wavelengths. Wright et al. (2009) listed 390 point sources detected at least at one frequency in WMAP five-year maps. The re-analysis by Massardi et al. (2009), using both blind and non-blind detection techniques, increased to 484 the number of detections with signal to noise ratio $\geq 5$, at $|b| > 5^\circ$. The completeness level at high Galactic latitudes is $\simeq 1$ Jy at 23 GHz, and increases somewhat at higher frequencies, to $\simeq 2$ Jy at 61 GHz.

The higher sensitivity and better angular resolution of LFI will allow a substantial progress. Applying a new multi-frequency linear filtering technique to realistic LFI simulations of the sky, Herranz et al. (2009) detected, with 95% reliability, 1600, 1550, and 1000 sources at 30, 44, and 70 GHz, respectively, over about 85% of the sky. The 95% completeness fluxes are 540, 340, and 270 mJy at 30, 44, and 70 GHz, respectively. For comparison, the total number of $|b| > 5^\circ$ sources detected by Massardi et al. (2009) at $\geq 5\sigma$ in WMAP 5-yr maps at 33, 41, and 61 GHz, including several possibly spurious objects, is 307, 301, and 161, respectively.

As illustrated by Fig. 6, the much bigger source sample expected from Planck will allow us to have good statistics for different sub-populations of sources, some of which are not or only poorly represented in the WMAP sample. We may note, in this respect, that high-frequency surveys will really open a window on extragalactic radio sources. Those dominating low-frequency surveys are characterized, primarily, by optically thin synchrotron emission and fade away at high frequencies. Much more complex physics shows up at high frequencies: electron ageing effects on optically thin emission, spectral peaks due to short-lived evolutionary phases, spectral steepening due to the transition of emission regions from the optically thick to the optically thin regime.

The dominant radio population at LFI frequencies are flat-spectrum radio quasars (FSRQs), for which LFI will provide a bright sample of $\geq$ 1000 objects, well suited to cover the parameter space of current physical models. Interestingly, the expected numbers of blazars and BL Lac objects detectable by

LFI are similar to those expected from the Fermi Gamma-ray Space Telescope (formerly GLAST; (Abdo 2009); (Fermi/LAT Collaboration: W. B. Atwood 2009)). It is likely that the LFI and the Fermi blazar samples will have a substantial overlap, making possible a much better definition of the relationships between radio and gamma-ray properties of these sources than has been possible so far.

The analysis of spectral properties of the ATCA 20 GHz bright sample indicates that quite a few high-frequency selected sources have peaked spectra. Most of them are likely aged beamed objects (blazars) whose radio emission is dominated by a single knot in the jet caught in a flaring phase. The Planck sample will allow us to get key information on the frequency and timescales of such flaring episodes, on the distribution of their peak frequencies, and therefore on the propagation of the flare along the jet. A small fraction of sources showing high frequency peaks may be extreme High Frequency Peakers (Dallacasa et al. 2000), thought to be newly born radio sources (ages as low as thousand years). Obviously, the discovery of just a few such sources would be extremely important to shed light on the poorly understood mechanisms that trigger the radio activity.

Spectral peaks at frequencies of tens of GHz are also associated to late phases of the evolution of Active Galactic Nuclei, characterized by low accretion/radiative efficiency (ADAF/ADIOS sources). Predictions on the counts of such sources are extremely uncertain, but according to some models (Pierpaoli & Perna 2004) LFI may detect a significant number of them. In any case, Planck will set important constraints on the space density of these sources.

WMAP has detected polarized fluxes at $\geq 4\,\sigma$ in two or more bands for only five extragalactic sources (Wright et al. 2009). LFI will substantially improve on that, providing polarization measurements for tens of sources, thus allowing us to get the first statistically meaningful unbiased sample for polarization studies at mm wavelengths. It should be noted that Planck polarization measurements will not be confusion limited, as in the case of total flux, but noise limited. Thus the detection limit for polarized flux in LFI channels will be $\simeq$ 100–200 mJy, i.e. substantially lower than for total flux.

As mentioned above, the astrophysics programme of Planck is much wider than that achievable with LFI alone, both for the specific role of HFI and, in particular, for the great scientific sinergy between the two instruments. As a remarkable example we mention below the Planck contribution to the astrophysics of clusters.

Planck will also detect thousands of galaxy clusters out to redshifts of order unity via their thermal Sunyaev-Zeldovich effect (Leach et al. 2008; Bartlett et al. 2008). This sample will be extremely important both to understand the formation of large scale structure and the physics of the intracluster medium. For such measurements, a broad spectral coverage, i.e. the combination of data from both Planck instruments (LFI and HFI), is a key asset. Such combination will allow, in particular, to accurately correct for the contamination from radio sources (mostly thanks to LFI channels) and from dusty galaxies (HFI channels) either associated to the clusters or in their foreground/background.

### *2.3. Scientific data analysis*

Data analysis for a high precision experiment such as LFI must provide reduction of the data volume by several orders of magnitude with minimal loss of information. The sheer size of the dataset, the weakness of the vast majority of the science targets, the significance of the statistical and systematic sources of error all conspire to make data analysis an all but trivial task.

The map making layer provides a lossless compression by several orders of magnitude, projecting the dataset from time domain to the discretized celestial sphere (Tegmark 1997). Furthermore, timeline-specific instrumental effects that are not scan synchronous get reduced in magnitude when projected from time to pixel space (see e.g. Mennella et al. (2002)) and, in general, the analysis of maps provides a more convenient mean to assess the level of systematics as compared to timeline analysis.

Several map making algorithms have been proposed to produce sky maps in total intensity (Stokes I) and linear polarization (Stokes Q and U) out of LFI timelines. So-called "destriping" algorithms have historically been proposed first. These take advantage of the details of the Planck scanning strategy to suppress correlated noise (Maino et al. 1999b). Although computationally efficient, these methods do not -in general- yield a minimum variance map. To overcome this problem, minimum variance map making algorithms have been devised and implemented specifically for LFI (Natoli et al. 2001; de Gasperis et al. 2005). The latter are also known as Generalized Least Squares (GLS) methods and are accurate and flexible. Their drawback is that, at Planck size, they require significant amount of massively power computational resources (Poutanen et al. 2006; Ashdown et al. 2007c,a) and are thus unfeasible to serve within a Monte Carlo context. To overcome the limitations of GLS algoithms the LFI community has developed ad-hoc hybrid algorithms **?**, which can perform as a destriper when this is desirable or appropriate, but can reach the accuracy of a GLS algorithm when a higher computational cost can be afforded. While, in the latter case, hybrid algorthms and GLS demand similar resources, unlike the GLS, the hybrid approach is user tunable to desired prescision. The baseline map making algorithms for LFI is an hybrid code dubbed `madam`.

Map making algothms can in general compute the correlation (inverse covariance) matrix of the map estimate they deliver **?**. At high resolution such a computation, though feasible, is unpractical, because the size of the matrix makes prohibitive its handling and inversion. At low resolution the covariance matrix will instead be produced, and it is of extreme importance for the accurate characterization of the low multipoles of the CMB **?**.

A key tier of Planck data analysis is the separation of astrophysical from cosmological components. A variety of methods have been developed to this extent. They can be grossly divided in two groups, depending on the nature of the prior information used. The so-called blind methods rely only on the statistical independence of background and foreground emissions, while non blind methods assume and exploit prior information about the physical modelling of the foreground. In either case, multi frequency data is necessary to achieve robust separation of the components. Non blind methods can be very effective when the prior information can be trusted. For total intensity, physical modelling of foreground emission rests on solid basis, and the choice of non blind methods appears well motivated. On the other hand, non blind algorithms are prone to bias and thus unfit when prior information is lacking or unreliable. For this reason, blind methods are likely to turn out a better choice for polarization.

The extraction of statistical information from the CMB usually proceeds via correlation functions. Since the CMB field is Gaussian to large extent (Smith et al. 2009b), most of the information is encoded in the two-point function or equivalently in its reciprocal representation in spherical harmonics space. Assuming rotational invariance, the latter quantity is well de-

scribed by the APS. For an ideal experiment, the estimated APS could be directly compared to a Boltzmann code prediction to constrain the cosmological parameters. However, in view of incomplete sky coverage (which induces couplings among multipoles) and the presence of noise (which, in general, is not rotationally invariant) a more accurate analysis is necessary. The likelihood function for a Gaussian CMB sky can be easily written and provide a sound mechanism to constrain models and data. The direct evaluation of such a function, however, poses untractable computational issues. Fortunately, only the lowest multipoles require exact treatment. This can be done either by direct evaluation using massively parallel computers or sampling the posterior distribution of the CMB using adequate methods, such as the Gibbs approach (Chu et al. 2005). At high multipoles, where the likelihood function cannot be evaluated exactly, a wide range of effective, computationally affordable approximations exist (see e.g. Hamimeche & Lewis (2008) and references therein).

## 3. Instrument

### 3.1. Optics

During the design phase of LFI, great effort has been dedicated to the optical design of the focal plane unit. As already mentioned in the Introduction, the actual design of the Planck telescope derives from COBRAS and has been further tuned by the subsequent studies of the LFI team (**?**) and Thales-Alenia Space. These pointed out the importance to increase the telescope diameter (Mandolesi et al. (????)), to optimize the optical design and also showed the complexity to match the real focal surface with the horn phase centre (Valenziano & Bersanelli (????)). The optical design of LFI is the result of a long iteration process in which the position and orientation of each feed horn has been optimized as a trade-off between angular resolution and sidelobe rejection levels (san (????)). Tight limits were also imposed by mechanical constraints. The 70 GHz system has been subject to a dedicated activity to improve the single horn design and its relative location in the focal surface. As a result the angular resolution has been maximized.

The feed horn development programme started in the early stages of the mission with prototype demonstrators (Bersanelli et al. (1998)), followed by the Elegant Bread Board (Villa et al. (2002)) and finally by the Qualification and Flight Models (Villa et al 2009). The horn design has a corrugated shape with a dual profile (Gentili et al. (2000)). This choice was a posteriori justified by the complexity of the focal plane and the need to respect the interfaces with HFI.

Each of the corrugated horns feeds an orthomode transducers (OMT) which splits the incoming signal in two orthogonal polarized components (**?**). Since the horns do not perturb the polarization state of the incoming wave, this technique allows LFI to measure a linear polrized component. Typical value of OMT cross polarization is about $-30$dB setting the spurious polarization of the LFI optical interfaces at a level of 0.001.

Table 3.1 reports the overall LFI optical characteristics as expected in flight (Tauber 2009). The reported edge taper (ET) quoted in Table 3.1 does not correspond to the measured ET on the mirror. The reported angular resolution is the average full width half maximum (FWHM) of all the channels at the same frequency. The cross polar discrimination (XPD) is the ratio between the antenna solid angle of the cross polar pattern and the antenna solid angle of the copolar pattern, both calculated within the solid angle of the $-3$dB contour. The Sub and Main reflector spillover are the fraction of power that reaches the horns without being intercepted by the main and sub reflectors respectively.

**Table 2.** LFI Optical performances. All the values are averaged over all channels at the same frequency. ET is the horn edge taper; FWHM is the angular resolution in arcmin; $e$ is the ellipticity; XPD is the cross polar discrimination in dB; Ssp is the Sub reflector spillover (%); Msp is the Main reflector spillover (%). See text for details.

| | ET | FWHM | $e$ | XPD | Ssp | Msp |
|---|---|---|---|---|---|---|
| 70 | 17dB22° | 13.03 | 1.22 | -34.73 | 0.17 | 0.65 |
| 44 | 30dB22° | 26.81 | 1.26 | -30.54 | 0.074 | 0.18 |
| 30 | 30dB22° | 33.34 | 1.38 | -32.37 | 0.24 | 0.59 |

### 3.2. Radiometers

LFI is designed to cover the low frequency portion of the wideband Planck all-sky survey. A detailed description of the design and implementation of the LFI instrument is given in Bersanelli et al. (2009) and references therein, while the results of the onground calibration and test campaign is presented in Mennella et al (2009) and Villa et al (2009). The LFI is an array of cryogenically cooled radiometers designed to observe in three frequency bands centered at 30 GHz, 44 GHz, and 70 GHz with high sensitivity and freedom from systematic errors. All channels are sensitive to the $I$, $Q$ and $U$ Stokes parameters thus providing information on both temperature and polarisation anisotropies. The heart of the LFI instrument is a compact, 22-channel multifrequency array of differential receivers with cryogenic low-noise amplifiers based on indium phosphide (InP) high-electron-mobility transistors (HEMTs). To minimise power dissipation in the focal plane unit, which is cooled to 20 K, the radiometers are split into two subassemblies (the front-end module, FEM, and back-end module, BEM) connected by a set of composite waveguides, as shown in Figure 1. Miniaturized, low-loss passive components are implemented in the front end for optimal performance and for compatibility with the stringent thermo-mechanical requirements in the interface with the HFI.

The radiometer design is driven by the need to suppress $1/f$-type noise induced by gain and noise temperature fluctuations in the amplifiers, which would be unacceptably high for a simple total power system. A differential pseudo-correlation scheme is adopted, in which signals from the sky and from a blackbody reference load are combined by a hybrid coupler, amplified in two independent amplifier chains, and separated out by a second hybrid (Figure 2). The sky and the reference load power can then be measured and differenced. Since the reference signal has been subject to the same gain variations in the two amplifier chains as the sky signal, the sky power can be recovered with high precision. Insensitivity to fluctuations in the back-end amplifiers and detectors is realized by switching phase shifters at 8 kHz synchronously in each amplifier chain. The rejection of $1/f$ noise as well as the immunity to other systematic effects is optimised if the two input signals are nearly equal. For this reason the reference loads are cooled to 4 K by mounting them on the 4 K structure of the HFI. In addition, the effect of the residual offset ($< 1$ K in nominal conditions) is reduced by introducing a gain modulation factor in the on-board processing to balance the output signal. As shown in Figure 2, the differencing receiver greatly improves the stability of the measured signal.

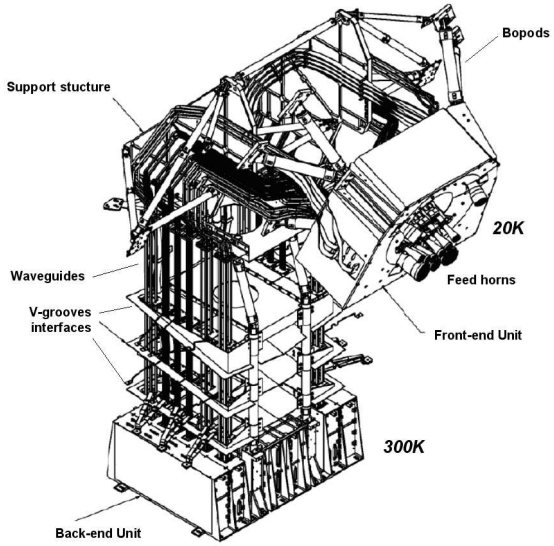


**Figure 7.** The LFI radiometer array assembly, with details of the front-end and back-end units. The front-end radiometers are based on wide-band low-noise amplifiers, fed by corrugated feedhorns which collect the radiation from the telescope. A set of compsite waveguides transport the amplified signals from the front-end unit (at 20 K) to the back-end unit (at 300 K). The waveguides are designed to meet simultaneously radiometric, thermal, and mechanical requirements, and are thermally linked to the three V-groove thermal shields of the Planck payload module. The back-end unit, located on top of the Planck service module, contains additional amplification as well as the detectors, and is interfaced to the data acquisition electronics. The HFI is inserted into and attached to the frame of the LFI focal-plane unit.

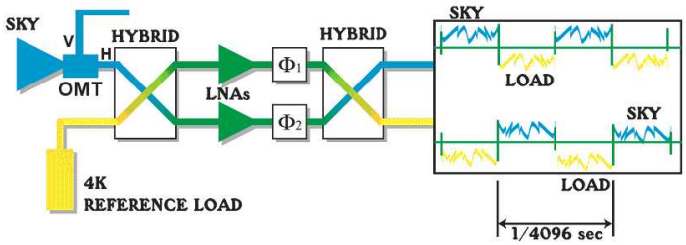


**Figure 8.** Schematic of the LFI front-end radiometer. The front-end unit is located at the focus of the Planck telescope, and comprises: dual profiled corrugated feed horns; low-loss (0.2 dB), wideband (> 20%) orthomode transducers; and radiometer front-end modules with hybrids, cryogenic low noise amplifiers, and phase switches.

The LFI amplifiers at 30 GHz and 44 GHz use discrete InP HEMTs incorporated into a microwave integrated circuit (MIC). At these frequencies the parasitics and uncertainties introduced by the bond wires in a MIC amplifier are controllable and the additional tuning flexibility facilitates optimization for low noise. At 70 GHz there will be twelve detector chains. Amplifiers at these frequencies will use monolothic microwave integrated circuits (MMICs), which incorporate all circuit elements and the HEMT transistors on a single InP chip. At these frequencies, MMIC technology provides not only significantly better performance than MIC technology, but also allows faster assembly and smaller sample-to-sample variance. Given the large number of amplifiers required at 70 GHz, MMIC technology can rightfully be regarded as enabling for the LFI.

Fourty-four waveguides connect the LFI front-end unit, cooled to 20 K by a hydrogen sorption cooler, to the back-end unit, which is mounted on the top panel of the Planck SVM and it is maintained at a temperature of 300 K. The BEU comprises the eleven BEMs and the data acquisition electronics (DAE) unit which provides adjustable bias to the amplifiers and phase switches as well as scienctific signal conditioning. In the back-end modules the the RF signals are further amplified in the two legs of the radiometers by room temperature amplifiers. The signals are then filtered and detected by square low detector diodes. A DC amplifier then boosts the signal output which is connected to the data acquisition electronics. After on-board processing, provided by the Radiometer Box Electronics Assembly (REBA), the compressed signals are downlinked to the ground station together with housekeeping data. The sky and reference load DC signals are transmitted to the ground as two separated streams of data to ensure optimal calculation of the gain modulation factor for minimal $1/f$ noise and systematic effects. The complexity of the LFI system called for a highly modular plan for testing and intergation. Performance verification was first carried out at single unit-level, followed by campaigns at sub-assembly and instrument level, then completed with full functional tests after integration in the Planck satellite. Scientific calibration has been carried out in two main campaigns, first on the individual radiometer chain assemblies (RCAs), i.e. the units comprising a feed horn and the two pseudo-correlation radiometers connected to each arm of the orthomode transducer (see Figure 2), and then at instrument level. For the RCA campaign we used sky loads and reference loads cooled near 4 K which allowed accurate verification of the instrument performances in near-flight conditions. Instrument level tests were carried out with loads at 20 K, which allowed to verify the radiometer performances in the integrated configuration. Testing at RCA and Instrument level, both for the qualification model (QM) and for the flight model (FM), were carried out at Thales Alenia Space, Vimodrone (Milano, Italy). Finally, system-level tests of the LFI integrated with HFI in the Planck satellite were carried out at CSL in the summer of 2008.

### *3.3. Sorption Cooler*

The Sorption Cooler Sub-system (SCS) is the first active element of the Planck cryochain. Its purpose is to cool the LFI radiometers down to their operational temperature around 20 K while providing a pre-cooling stage for the HFI cooling system: a 4.5 K mechanical Joule-Thomson cooler and a Benoit style open cycle dilution refrigerator. Two identical sorption coolers have been fabricated and assembled by Jet Propulsion Laboratory (JPL) under a contract with NASA. JPL has been a pioneer in the development and application of such cryocoolers for space and the two Planck units are the first continuous closed cycle hydrogen sorption coolers to be used for a space mission (Morgante 2009b).

Sorption refrigerators are attractive systems for cooling instruments, detectors and telescopes when a vibration free system is required. Since pressurization and evacuation is accomplished simply by heating and cooling the sorbent elements sequentially, with no moving parts, they tend to be very robust and, essentially, generate no vibrations on the spacecraft. This provides excellent reliability and long life. Also, cooling by Joule-Thomson (J-T) expansion through orifices, the cold end can be located remotely (thermally and spatially) from the warm end. This allows for excellent flexibility in integration of the cooler to the cold payload and the warm spacecraft.

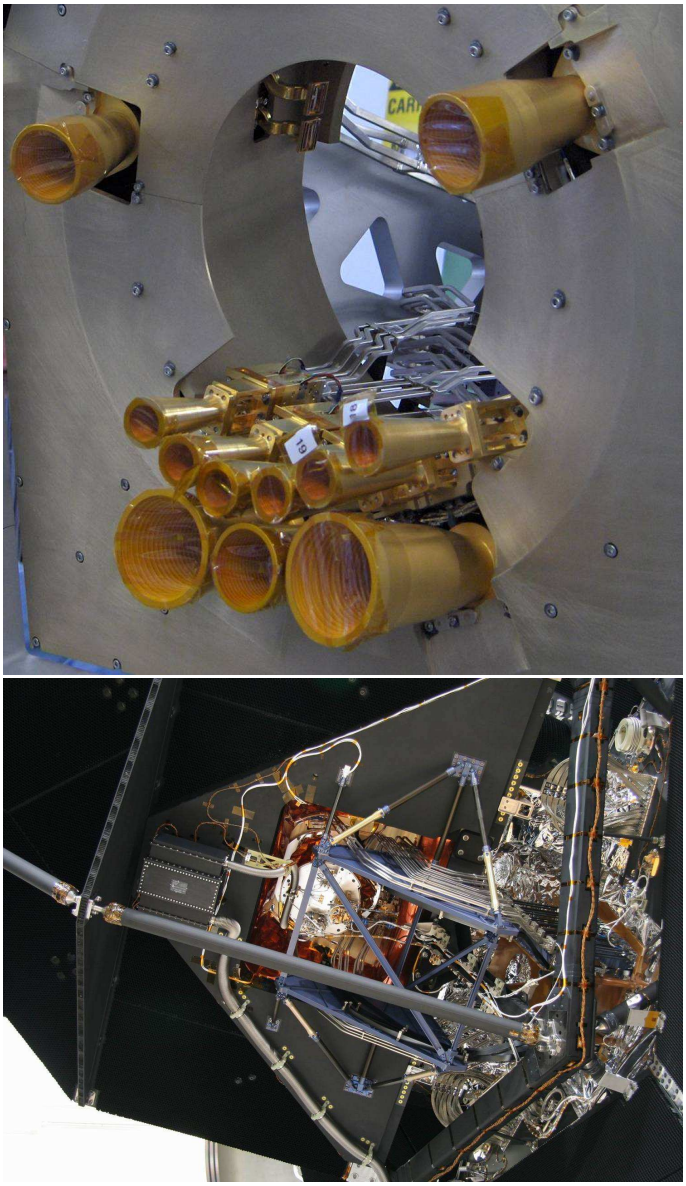

**Figure 9.** Top panel: picture of the LFI focal plane showing the feed-horns and main frame. The central portion of the main frame is designed to provide the interface to the HFI front-end unit, where the reference loads for the LFI radiometers are located and cooled to 4K. Bottom panel: A back-view of the LFI integrated on the Planck satellite. Visible are the upper sections of the waveguides interfacong the front-end unit, as well as the mechanical support structure.

#### 3.3.1. Specifications

The main requirements of the Planck SCS can be summarized below:

- Provide about 1 W total heat lift at instrument interfaces using a ≤ 60 K pre-cooling temperature at the coldest V-groove radiator on the Planck spacecraft
- Maintain the following instrument interfaces temperatures:
  - LFI at ≤ 22.5 K [80% of total heat lift]
  - HFI at ≤ 19.02 K [20% of total heat lift]
- Temperature stability (over its operating period ≈ 6000 s):
  - ≤ 450 mK, peak-to-peak at HFI interface
  - ≤ 100 mK, peak-to-peak at LFI Interface
- Input power consumption ≤ 470 W (at end of life, excluding electronics)
- Operational lifetime: ≥ 2 years (including testing)

#### 3.3.2. Operations

The SCS is composed of a Thermo-Mechanical Unit (TMU, see Fig. 10) and electronics to operate the system. Cooling is produced by J-T expansion with hydrogen as the working fluid. The key element of the 20 K sorption cooler is the Compressor, an absorption machine that pumps hydrogen gas by thermally cycling six compressor elements (sorbent beds). The principle of operation of the sorption compressor is based on the properties of a unique sorption material (a La, Ni and Sn alloy), which can absorb a large amount of hydrogen at relatively low pressures, and desorb it to produce high-pressure gas when heated in a limited volume. Electrical resistances accomplish heating of the sorbent while the cooling is achieved by thermally connecting, via gas-gap thermal switches, the compressor element to a warm radiator at 270 K on the satellite Service Module (SVM). Each sorbent bed is connected to both the high pressure and low-pressure sides of the plumbing system through check valves, which allow gas flow in a single direction only. To damp out oscillations on the high-pressure side of the compressor, a High-Pressure Stabilization Tank (HPST) system is utilized. On the low-pressure side, a Low-Pressure Storage Bed (LPSB) filled with hydride, primarily operates as a storage bed for a large fraction of the $H_2$ inventory required to operate the cooler during flight and ground testing while minimizing the pressure in the non-operational cooler during launch and transportation. The compressor assembly mounts directly onto the Warm Radiator (WR) on the spacecraft. As each sorbent bed is taken through four steps (heat up, desorption, cool-down, absorption) in a cycle, it will intake low-pressure hydrogen and output high-pressure hydrogen on an intermittent basis. In order to produce a continuous stream of liquid refrigerant the sorption beds phases are staggered so that at any given time, one is desorbing while the others are heating up, cooling down, or re-absorbing low-pressure gas.

The compressed refrigerant then travels in the Piping and Cold End Assembly (PACE, see Fig. 10), through a series of heat exchangers linked to three V-Groove radiators on the spacecraft which provide passive cooling down to approximately 50 K. Once pre-cooled to the required range of temperatures, the gas is expanded through the J-T valve. Upon expansion, hydrogen forms liquid droplets whose evaporation provides the cooling power. The liquid/vapour mixture then sequentially flows through the two Liquid Vapour Heat eXchangers (LVHX) inside the cold end. LVHX1 and 2 are thermally and mechanically linked to the corresponding instrument (HFI and LFI) interface. The LFI is coupled to the LVHX2 through an intermediate thermal stage, the Temperature Stabilization Assembly (TSA). A feedback control loop (PID type), operated by the cooler electronics, is able to control the TSA peak-to-peak fluctuations down to the required level (≤100 mK). Heat from the instruments evaporates liquid hydrogen and the low pressure gaseous hydrogen is circulated back to the cold sorbent beds for compression.

#### 3.3.3. Performance

The two flight sorption cooler units have been delivered to ESA in 2005. Prior to delivery, in early 2004, both flight models underwent sub-system level thermal vacuum test campaigns at JPL. In spring 2006 and summer 2008 respectively, SCS Redundant

| SCS Unit | Warm Rad T (K) | 3 rd VGroove T (K) | Cold End T (K) HFI I/F | LFI I/F | Heat Lift (mW) | Input Power (V) | Cycle Time (s) |
|---|---|---|---|---|---|---|---|
| Redundant | 270.5 | 45 | 17.2 | 18.7 [a,b] | 1100 | 297 | 940 |
| | 277 | 60 | 18.0 | 20.1 [a,b] | 1100 | 460 | 492 |
| | 282.6 | 60 | 18.4 | 19.9 [a,b] | 1050 | 388 | 667 |
| Nominal | 270 | 47 | 17.1 | 18.7 [a] | 1125 | 304 | 940 |
| | 273 | 48 | 17.5 | 18.7 [a] | N/A [c] | 470 | 525 |

[a] Measured at Temperature Stabilization Assembly (TSA) stage
[b] In SCS-Redundant test campaign TSA stage active control was not enabled
[c] Not measured

**Table 3. SCS flight units performance summary.**

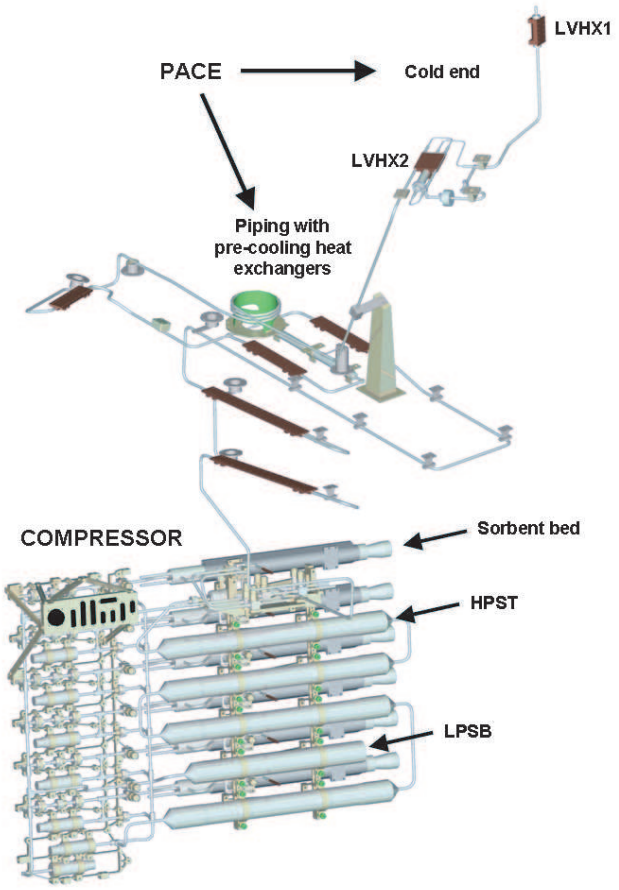


**Figure 10.** SCS Thermo-Mechanical Unit.

and Nominal have been tested in cryogenic conditions on the spacecraft FM at the Centre Spatial de Liege (CSL) facilities. Results from these two major test campaigns are summarized in Table 3.3.2 and reported in full detail in Morgante (2009b).

## 4. LFI Programme

The model philosophy adopted for LFI and the SCS was chosen to meet the requirements of the ESA Planck System which assumed from the beginning that there would be three development models of the satellite:

– The Planck Avionics Model (AVM) inwhich the System Bus was shared with the Herschel satellite, and allowed basic electrical interface testing of all units and communication protocol and software interface verification.
– The Planck Qualification Model (QM) which was limited to the Planck Payload Module (PPLM) containing QMs of LFI, HFI, and the Planck telescope and structure that would allow a qualification vibration test campaign to be performed at payload level, alignment checks, and would inparticular allow a cryogenic qualification test campaign to be performed on all the advanced instrumentation of the payload that had to fully perform in cryogenic conditions.
– The Planck Protoflight Model (PFM) which contained all the Flight Model (FM) hardware and software that would undergo the PFM environmental test campaign culminating in extended thermal and cryogenic functional performance tests.

### *4.1. Model Philosophy*

In correspondence with the system model philosophy it was decided by the Planck Consortium to follow a conservative incremental approach containing Prototype Demonstrators.

#### 4.1.1. Prototype Demonstrators PDs)

The scope of the PDs was to validate the LFI radiometer design concept giving early results on intrinsic noise, particularly $1/f$ noise properties, and characterise in a preliminary fashion systematic effects to give requirement inputs for the rest of the instrument design and at satellite level. The PDs also gave the advantage of being able to test and gain experience with very low noise HEMT amplifiers, hybrid couplers, and phase switches. The PD development started early in the programme during the ESA development Pre-Phase B activity and ran in parallel with the successive instrument development phase of elegant bread boarding.

#### 4.1.2. Elegant Breadboarding (EBB)

The fundamental purpose of the LFI EBBs was to demonstrate full radiometer design maturity prior to initiating qualification model build over the whole frequency range of LFI. Thus full continuous comparison radiometers (2 channels and thus covering a single polarisation direction) were constructed centred on 100 GHz, 70 GHz, and 30 GHz running from their expected design of the corrugated feed-horns at the their entrance back as far as their expected design diode output stages at their back-end. These were put through thorough functional and performance tests with their front end sections operating at 20 K as expected in flight. It was towards the end of this development that the financial difficulties which terminated the 100 GHz channel development hit the programme.

#### 4.1.3. The QM

The development of the LFI QM commenced in parallel with the EEB activities. From the very beginning it was decided that only a limited number of radiometer chain assemblies (RCA) each containing 4 radiometers and thus covering fully two orthogonal polarisation directions) at each frequency should be included and that the remaining would be represented by thermal mechanical dummies. Thus the LFI QM contained 2 RCA at 70 GHz and one each at 44 GHz and 30 GHz. The active components of the Data Acquisition Electronics (DAE) were thus dimensioned accordingly. The Radiometer Electronics Box Assembly (REBA) QM supplied was a full unit. All units and assemblies went through approved unit level qualification level testing prior to integration as the LFI QM in the facilities of the instrument prime contractor Thales Alenia Space Milano.

The financial difficulties that have already been mentioned also disrupted QM development and lead to a thermal-mechanical representative dummy of LFI being employed by ESA in the system level satellite QM test campaign because of the ensuing delay in the availability of the LFI QM. The LFI QM was however fundamental in the development of LFI as it gave the LFI Consortium the opportunity to perform representative cryo-testing of a reduced model of the instrument and thus confirm the design of the LFI flight Model.

#### 4.1.4. The FM

The LFI FM contained flight standard units and assemblies that went through flight unit acceptance level tests prior to integration as the LFI FM. In addition prior to mounting in the LFI FM each RCA went through a separate cryogenic test campaign after assembly to allow preliminary tuning to achieve best performance and confirm the overall functional performance of each radiometer. At the LFI FM test level the instrument went through an extended cryogenic test campaign that included a further level of tuning and the instrument calibration that could not be performed when mounted in the final configuration on the satellite because of schedule and cost constraints. At the time of delivery of the LFI FM to ESA for integration on the satellite the only significant verification test that remained to be done was the vibration testing of the fully assembled Radiometer Array Assembly (RAA) that could not be done in a meaning-full way at instrument level because of the problem of simulating the coupled vibration input through the DAE and the LFI FPU mounting in to the RAA (and in particular in to the waveguides). This verification was completed successfully during the satellite PFM vibration test campaign.

#### 4.1.5. The AVM

The LFI AVM was composed of the DAE QM, and its secondary power supply box removed from the RAA of the LFI QM, an AVM model of the REBA and the QM instrument harness. No radiometers were present in the LFI AVM, and their active inputs on the DAE were terminated with resistors. The LFI AVM was used successfully by ESA in the Planck System AVM test campaigns to fulfil its scope outlined above.

### *4.2. The SCS Model Philosophy*

The SCS model development was designed to produce two coolers a nominal cooler and a redundant cooler. The early part of the model philosophy adopted was similar to that of LFI employing prototype development and testing of key components such as single compressor beds prior to the building of an EBB containing a complete compliment of components as in a cooler intended to fly. This EBB cooler was submitted to an intensive functional and performance test campaign. The Sorption Cooler Electronics (SCE) meanwhile started development with an EBB and was followed by a QM and then FM1/FM2 build.

The TMUs of both the nominal and redundant sorption coolers went through protoflight unit testing prior to assembly with their respective PACE for thermal/cryogenic testing before delivery. To conclude the qualification of the PACE a spare unit participated in the PPLM QM system level vibration and cryogenic test campaign.

An important constraint in the ground operation of the sorption coolers is that they could not be fully operated with their compressor beds far from a horizontal position. This was to avoid permanent non homogeneity in the distribution of the hydrides in the compressor beds and the ensuing loss in efficiency. In the fully integrated configuration of the satellite, the PFM thermal and cryogenic test campaign, for test chamber configuration, schedule and cost reasons would allow only one cooler to be in a fully operable orientation. Thus the first cooler to be supplied, which was designated the redundant cooler (FM1), was mounted with the PPLM QM and put through a cryogenic test campaign (termed PFM1) with similar characteristics to those of the final thermal balance and cryogenic tests of the fully integrated satellite prior to integration in the satellite where only short fully powered health checking would be done on it. The second cooler was designated as the nominal cooler (FM2) and participated fully in the final cryo-testing of the satellite. For both coolers final verification (TMU assembled with PACE) was achieved during the Planck system level vibration test campaign and subsequent tests.

The AVM of the SCS was supplied using the QM of the SCE and a simulator of the TMU to simulate the power load of a real cooler.

### *4.3. System Level Integration and Test*

The Planck satellite together with the instruments was integrated in the Thales Alenia Space facilities at Cannes in France.

The SCS nominal and redundant coolers were integrated on to the Planck satellite before LFI and HFI.

Prior to integration on the satellite, the HFI FPU was integrated in to the FPU of LFI. This involved mounting the LFI 4K-Loads on HFI before starting the main integration process which was a very delicate operation considering that when done the closest approach of LFI and HFI would be of the order of 2 mm. It should be remembered that LFI and HFI had not “met” during the Planck QM activity and so this integration was performed for the first time during the Planck PFM campaign. The integration process had undergone much study and required a special rotatable GSE for the LFI RAA, and a special suspension and balancing system to allow HFI to be lifted and lowered in to LFI at the correct orientation along guide rails from above. Fortunately the integration was completed successfully.

Subsequently the combined LFI RAA and HFI FPU were integrated on to the satellite supported by the LFI GSE which was eventually removed during integration to the telescope. The process of electrical integration and checkout was then completed for LFI, the SCS and HFI, and the Proto-Flight Model test campaign was commenced.

For LFI this test campaign proceeded with ambient functional checkout followed by detailed tests as a complete sub-

system prior to participation with the SCS and HFI in the sequence of alignment, EMC, sine and acoustic random vibration tests, and the sequence of system level verification tests with the Mission Operations Control Centre (MOC at ESOC, Darmstadt) and LFI DPC. During all these tests, at key points, both the nominal and redundant SCS were put through ambient temperature health checks to verify basic functionality.

The environmental test campaign culminated with the thermal balance and cryogenic tests carried out in the Focal 5 facility of the Centre Spatial de Liege, Belgium. The test was designed to follow very closely the expected cool-down scenario after launch through to normal mission operations and it was during these tests that the two instruments and the Sorption Cooler directly demonstrated together not only their combined capabilities but also their operational margins with success.

## 5. LFI test and verification

The LFI has been tested and calibrated before launch at various levels of integration, from the single components up to instrument and satellite levels; this approach, which is summarised schematically in Fig. 11, provided inherent redundancy and optimal instrument knowledge.

Passive components, i.e. feed-horns, OMTs and waveguides, have been tested at room conditions at the Plasma Physics Institute of the National Research Council (IFP-CNR) using a Vector Network Analyser. A summary of the measured performance parameters is provided in Table 4; measurements and results are discussed in detail in Villa et al. (2009c,b); D'Arcangelo et al. (2009).

**Table 4.** Measured performance parameters of the LFI passive components.

| | |
|---|---|
| **Feed Horns** | Insertion Loss, Return Loss, Cross-polar (±45°) and Co-polar patterns (E, H and ±45° planes) in amplitude and phase, Edge taper at 22° |
| **OMTs** | Insertion Loss, Return Loss, Cross-polarisation, Isolation |
| **Waveguides** | Insertion Loss, Return Loss |

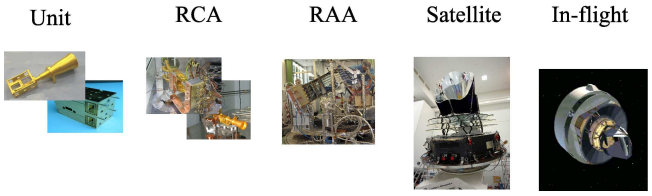


**Figure 11.** Schematic of the various calibrations steps in the LFI development.

Also radiometric performances were measured several times during the LFI development on individual sub-units (amplifiers, phase switches, detector diodes, etc.) on integrated front-end and back-end modules (Davis et al. 2009; Artal et al. 2009; Varis et al. 2009) and on the complete radiometric assemblies both as independent RCAs (Villa et al. 2009a) and in RAA, the final integrated instrument configuration (Mennella et al. 2009).

In Table 5 (taken from Mennella et al. (2009)) we list the main LFI radiometric performance parameters and the integration levels at which they have been measured. After the flight instrument test campaign the LFI has been cryogenically tested again after integration on the satellite with the HFI while the final characterisation will be performed in flight before starting nominal operations.

**Table 5.** Main calibration parameters and where they have been / will be measured. The following abbreviations have been used: SAT = Satellite, FLI = In-flight, FE = Front-end, BE = Back-end, LNA = Low Noise Amplifier, PS = Phase Switch, Radiom = Radiometric, Susc = Susceptibility.

| Category | Parameters | RCA | RAA | SAT | FLI |
|---|---|---|---|---|---|
| ***Tuning*** | FE LNAs | Y | Y | Y | Y |
| | FE PS | Y | Y | Y | Y |
| | BE offset and gain | Y | Y | Y | Y |
| | Quantisation / compression | N | Y | Y | Y |
| ***Radiom.*** | Photometric calibration | Y | Y | Y | Y |
| | Linearity | Y | Y | N | N |
| | Isolation | Y | Y | N | N |
| | In-band response | Y | N | N | N |
| ***Noise*** | White noise | Y | Y | Y | Y |
| | Knee freq. | Y | Y | Y | Y |
| | $1/f$ slope | Y | Y | Y | Y |
| ***Susc.*** | FE temperature fluctuations | Y | Y | Y | Y |
| | BE temperature fluctuations | Y | Y | N | N |
| | FE bias fluctuations | Y | Y | N | N |

RCA and RAA test campaigns have been key to characterise the instrument functionality and behaviour, and measure its expected performance in flight conditions. In particular 30 GHz and 44 GHz RCAs have been integrated and tested in Italy, at the Thales Alenia Space (TAS-I) laboratories in Milan, while the 70 GHz RCA test campaign has been carried out in Finland at the Yilinen-Elektrobit laboratories (Villa et al. 2009a). After this testing phase the 11 RCAs have been collected and integrated with the flight electronics in the LFI main frame at the TAS-I labs where the instrument final test and calibration has taken place (Mennella et al. 2009). Custom-designed cryofacilities (Terenzi et al. 2009b; Morgante 2009a) and high-performance black-body input loads (Terenzi et al. 2009a; Cuttaia et al. 2009) have been developed in order to test the LFI in the most flight-representative environmental conditions.

A particular point must be made about the front-end bias tuning which is a key step in setting the instrument scientific performances. Tight mass and power constraints called for a simple design of the DAE box so that power bias lines have been divided in five common-grounded power groups with no bias voltage readouts. Only the total drain current flowing through the front-end amplifiers is measured and is available in the housekeeping telemetry.

This design has important implications on front-end bias tuning, which depends critically on the satellite electrical and thermal configuration. Therefore this step has been repeated at all integration stages and will also be repeated during ground satellite

tests and in flight before the start of nominal operations. Details about bias tuning performed on front-end modules and on the individual integrated RCAs can be found in Davis et al. (2009), Varis et al. (2009) and Villa et al. (2009a).

Parameters measured on the integrated instrument have been found essentially in line with measurements performed on individual receivers; in particular the LFI shows excellent $1/f$ stability and rejection of instrumental systematic effects. On the other hand the very ambitious sensitivity goals have not been fully met and the white noise sensitivity (see Table 6) is ∼30% higher than requirements, the measured performances make LFI the most sensitive instrument of its kind, a factor of 2 to 3 better than WMAP at the same frequencies.

**Table 6.** Calibrated white noise from ground test results extrapolated at CMB input signal level. Two different methods are used here to provide a reliable range of values (see Mennella et al. (2009) for further details). The final verification of sensitivity will be derived in flight during the CPV phase.

| Frequency channel | 30GHz | 44GHz | 70GHz |
|---|---|---|---|
| White noise per $\nu$ channel $[\mu\mathrm{K}\cdot\sqrt{\mathrm{s}}]$ | 141÷154 | 152÷160 | 130÷146 |

## 6. LFI Data Processing Center

In order to take maximum advantage of the capabilities of the Planck mission and to achieve its very ambitious scientific objectives, proper data reduction and scientific analysis procedures were defined, designed, and implemented very carefully. The data processing was optimized so as to extract the maximum amount of useful scientific information from the data set and to deliver the calibrated data to the broad scientific community within a rather short period of time. As demonstrated by many previous space missions using state-of-the-art technologies, the best scientific exploitation is obtained by combining the robust, well-defined architecture of a data pipeline and its associated tools with the high scientific creativity essential when facing unpredictable features of the real data. Although many steps required for the transformation of data can and must be defined early in the development of the pipeline (most of the foreseeable ones have already been tested and implemented in the simulations made by the teams of both Consortia), some of them will remain unknown until flight data are obtained.

Planck is a PI mission, and its scientific achievements will depend critically on the performance of the two instruments, LFI and HFI, on the cooling chain, and on the telescope. The data processing will be performed by two Data Processing Centres (DPCs) (Pasian et al. 2000; Pasian & Gispert 2000; Pasian & Sygnet 2002). However, despite the existence of two separate distributed DPCs, the success of the mission relies heavily on the combination of the measurements from both instruments.

The development of the LFI DPC software has been performed in a collaborative way across a consortium spread across over 20 institutes in a dozen countries. Individual scientists belonging to the Software Prototyping Team develop prototype code, which is then delivered to the LFI DPC Integration Team. The latter is responsible to integrate, optimize and test the code, and has produced the pipeline software to be used during operations. This development takes advantage of tools defined within the Planck IDIS (Integrated Data and Information System) collaboration.

A software policy has been defined, with the aim of allowing the DPC to run the best possible algorithms within its pipeline, while fostering collaboration inside the LFI Consortium and across Planck, and preserving at the same time the intellectual property of the code authors on the processing algorithms devised.

The Planck DPCs are responsible for the delivery and archiving of the following scientific data products, which are the deliverables of the Planck mission:

- Calibrated time series data, for each receiver, after removal of systematic features and attitude reconstruction.
- Photometrically and astrometrically calibrated maps of the sky in the observed bands.
- Sky maps of the main astrophysical components.
- Catalogues of sources detected in the sky maps of the main astrophysical components.
- CMB Power Spectrum coefficients.

Additional products, necessary to the total understanding of the instrument, are being negotiated for inclusion in the Planck Legacy Archive (PLA). The products foreseen to be added to the formally defined products mentioned above are:

- Data sets defining the estimated characteristics of each detector and the telescope (e.g. detectivity, emissivity, time response, main beam and side lobes, etc. ...).
- "Internal" data (e.g. calibration data sets, data at intermediate level of processing);
- Ground Calibration and AIV Databases produced during the instrument development; and gathering all information, data and documents relative to the overall payload and all systems and sub-systems. Most of this information is crucial for processing flight data and updating the knowledge and the performances of the instrument.

The LFI DPC processing can be logically divided in three levels:

- Level 1: includes the Time Ordered Information (TOI) generation (a set of ordered information on a temporal basis or scan-phase basis). The current definition of the DPC product foresees the Real Time Assessment (RTA) and Quick Look Analysis (QLA) packages be integrated into the Level 1
- Level 2: TOIs produced at Level 1 will be cleaned up by taking away noise and many other types of systematic effects on the basis of calibration information. The final product of the Level 2 includes "frequency maps".
- Level 3: "Component maps" will come out from this level through a decomposition of single "frequency maps" using also products from the other instrument.

One additional level (Level S) used to develop the most sophisticated simulation based on real parameters extracted during ground test campaign, was also implemented. All these levels make use, inside the LFI DPC, of a pre-defined software infrastructure developed inside the IDIS collaboration.

We describe in the following sections the DPC Levels and the software infrastructure, and we finally report briefly on the tests that were applied to ensure that all pipelines are ready for the launch.

### 6.1. DPC Level 1

Level 1 takes input from the MOC's (Mission Operation Center) Data Distribution System (DDS), decompresses the raw data,

Calculated on the final resolution element per unit integration time

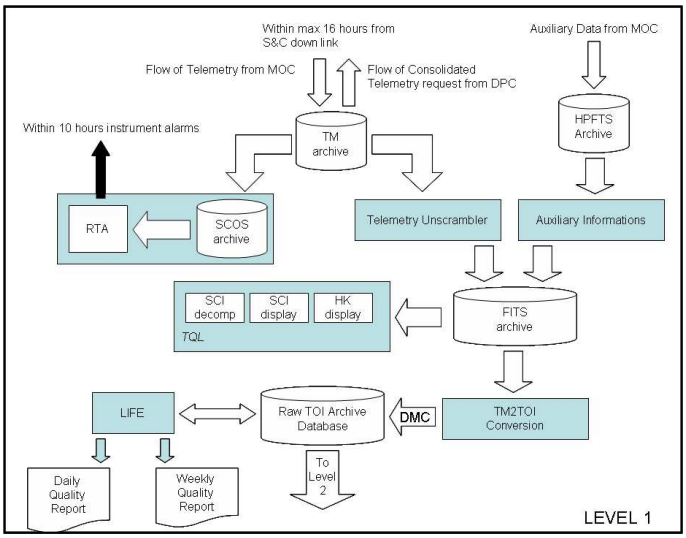


**Figure 12.** Level 1 structure.

and outputs Time Ordered Information for Level 2. Level 1 does not include scientific processing of the data; actions are performed automatically by using pre-defined input data and information from the technical teams. The input to Level 1 are telemetry (TM) and auxiliary data as they are released by the MOC. Level 1 uses TM data for performing a routine analysis (RTA - Real Time Assessment) of the Spacecraft and Instrument status, in addition to what is performed at the MOC, with the aim of monitoring the overall health of the payload and detecting possible anomalies, and performing a quick-look data analysis (TQL - Telemetry Quick Look) of the science TM to monitor the operation of the observation plan and to verify the behaviour of the instrument. The processing is meant to lead to the full mission raw-data stream in a form suitable for subsequent data processing by the DPC.

Level 1 deals also with all activities related to the production of reports. This task includes the results of telemetry analysis, but also the results of technical processing carried out on Time-Ordered Information (TOI) to understand the current and foreseen behaviour of the instrument. This second item includes specific analysis of instrument performance (LIFE - LFI Integrated perFormance Evaluator), and more general checking of time series (TSA - Time Series Analysis) for trend analysis purposes and comparison with the TOI from the other instrument. Additional tasks of Level 1 relate to its role of instrument control and DPC interface with the MOC. In particular, the following actions are performed:

- Preparation of telecommanding procedures aimed at modifying the instrument setup.
- Preparation of instrument database (MIBs).
- Communicate to the MOC "longer-term" inputs deriving from feedback from DPC processing.

In Level 1 all actions are planned to be performed on a "day-to-day" basis during observation. In Fig. 12 the structure of Level 1 and time required is reported. For more details refer to (Zacchei et al. 2009).

### 6.2. DPC Level2

At this level data processing steps requiring detailed instrument knowledge (data reduction proper) will be performed. The raw time series from Level 1 will be also used for reconstructing a number of sets of calibrated scans per each detector, as well as instrumental performances and properties, and maps of the sky for each channel. The processing is iterative, since simultaneous evaluation of quite a number of parameters should be made before the astrophysical signal can be isolated and averaged over all detectors in each frequency channel. Continuous exchange of information between the two DPCs, will be necessary at Level 2 in order to identify any suspect or unidentified behaviour or any results from the detectors.

The first task that the level 2 perform is the creation of differenced data. Level 1 stores data from both Sky and Load. These two have to be properly combined to produce differenced data therefore reducing the impact of 1/f noise. This is done via the computation of the so-called gain modulation factor "R" which is derived taking the ratio of the mean signals from both Sky and Load.

After differenced data are produced, the next step is the photometric calibration which transforms the digital unit in physical units. This operation is quite complex: different methods are implemented in the Level 2 pipeline that use the CMB dipole as an absolute calibrator allowing to convert data into physical units.

Another major task is beam reconstruction, which is implemented using information from planets crossing. We developed an algorithm performing a bi-variate approximation of the main beam section of the antenna pattern and reconstructing the position of the horn in the focal plane and its orientation with respect to a reference axis.

The step following the production of calibrated timelines is the creation of calibrated frequency maps. In order to do this, pointing information will be encoded into Time-Ordered Pixels i.e. pixel numbers in the given pixelisation scheme (HEALPix) identifying a given pointing direction ordered in time. In order to produce temperature maps it is necessary to reconstruct the beam pattern for the two polarization directions for the main, intermediate and far part of the beam pattern. This will allow to combine the two orthogonal components into a single temperature timeline. On this temperature timeline a map-making algorithm will be applied to produce a receiver map.

The instrument model allows to check and control systematic effects, quality of the removal performed by map-making and calibration of the receiver map. Receiver maps cleaned from systematic effects at different levels of accuracy will be stored into a calibrated maps archive. The production of frequency calibrated maps is done processing together all receivers from a given frequency channel in a single map-making run. In Figures 13 and 14 we report the steps performed by the Level 2 with the foreseen time associated.

### 6.3. DPC Level 3

The main task of the DPC Level 3 is the production of the maps for the different astrophysical and cosmological components present in the sky signal. From the reconstructed CMB component from component separation algorithms (or from a suitable linear combination and/or masking of the original calibrated frequency maps) the angular power spectrum of the CMB is computed for both temperature modes (TT) as well as polarization and cross temperature/polarisation modes.

The separation algorithms which will be exploited belong to two main categories, operating by means of priors on the signals to recover (non-blind), or relying on the statistical independence of the background and foreground emission (blind). Their domain of relevance are expected to be different for total intensity

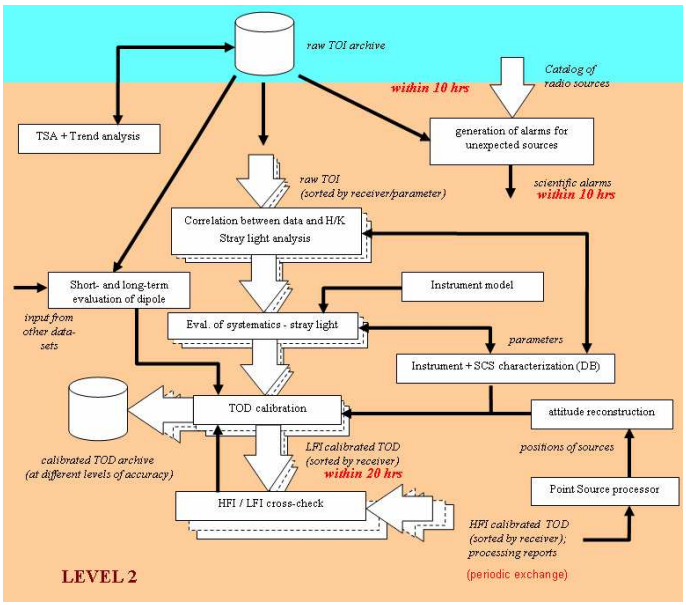


**Figure 13.** Level 2 Calibration pipeline.

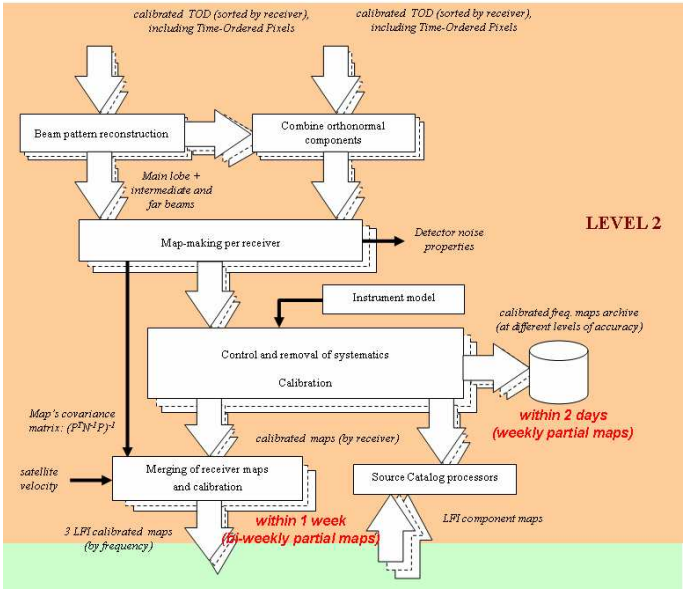


**Figure 14.** Level 2 MapMaking pipeline.

and polarization. Both blind and non-blind techniques require that the different emission processes superposed in the data feature a different behaviour with frequency. While the non-blind category requires to know in advance the coefficients scaling each signal at each frequency, the blind approach is capable to reconstruct the same scaling and does not need it as an input. In total intensity, a non-blind approach is reliable and achievable by means of the priors on the foreground which exist in the microwave band as well as outside. On the other hand the final results are biased by the constraints imposed. A blind approach represents most unbiased, being able to extract components which are uncorrelated with the others. That is therefore most appropriate for CMB extraction. In polarization, the lack of reliable priors may make the non-blind approach impossible, and a blind pipeline may be the only viable. Wiener filter and Maximum Entropy have been proposed in the literature and

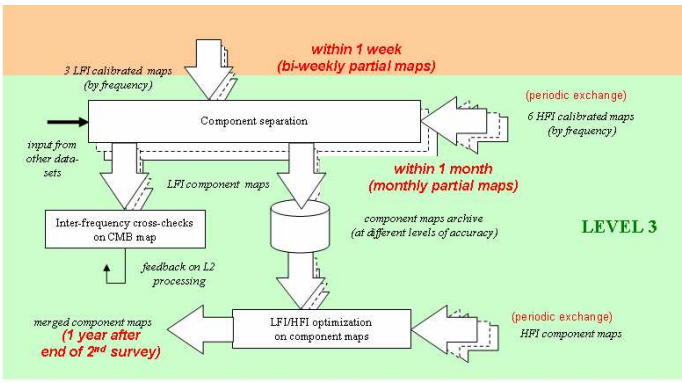


**Figure 15.** Level 3 pipeline structure.

were exploited in the non-blind category. The core of the blind approach is the Independent Component Analysis technique.

The inputs of the level 3 pipeline are the 3 calibrated receiver maps from LFI together with the 6 calibrated HFI frequency maps that are planned to be exchanged on a monthly basis. This is a crucial point: due to the great advantage of exploiting the full range of frequencies covered by Planck, the two DPCs have to work with the full set of calibrated maps (both LFI and HFI) in order to fully exploit the performance of the component separation tools. The Level 3 pipeline has deep links with most of the stages of Level 1 and Level 2. Systematic effects appearing in the TODs, source catalogues, noise distribution and statistics are all examples of important inputs and information to the component separation process. On the basis of that knowledge a confidence interval, or faithfulness criterium for CMB and foreground reconstruction can be built.

The main targets of the Level3 pipeline are two: one is the most faithful reconstruction of the CMB total intensity primary anisotropy pattern; the other is the weakening of the foreground contamination in polarization, allowing to fully exploit Planck to detect/pose upper limits on the existence of cosmological gravitational waves.

Level 3 will produce optimized component maps that will be delivered to the Planck Legacy Archive (PLA) with other information and data needed for the public release of the Planck products. As for power spectrum estimation Level 3 implements two independent and complementary approaches: a Monte-Carlo method suitable for high multipoles (based on the MASTER approach but including cross-power spectra from independent receivers) and a maximum-likelihood method for low multipoles. The combination of the two produce the final estimation of the angular power spectrum from LFI data. Combining LFI with HFI data where CMB is the dominant source of the sky emission, will produce in a similar manner the complete Planck CMB angular power spectrum. It is clear in this last stage of data processing that a complete knowledge of both instrument is essential for the extraction of an un-biased power spectrum. Therefore all the basic instrumental properties (beam shapes and width, noise spectra) should be properly and accurately known and accounted for. In Fig. 15 we report the step performed by the Level 3 with the foreseen time associated.

### *6.4. DPC Level S*

It was widely agreed within both Consortia that a strong need of software able to simulate the instrument footprint, starting from a predefined sky, was indispensable for the full period of the

Planck mission. Based on that idea the Level S was developed and as soon the knowledge of the instrument grew the Level S was developed in agreement (Reinecke et al. 2006). It includes all the instrument characteristics as they were understood during the ground test campaign. Simulated data were used to evaluate the performance of data-analysis algorithms and software vs the scientific requirements of the mission and to demonstrate the capability of the DPCs to work using blind simulations that contain unknown parameter values to be recovered by the data processing pipeline.

### 6.5. DPC Software Infrastructure

During the whole of the Planck mission it was necessary to deal with aspects related to information management, which pertain to a variety of activities concerning the whole project, ranging from instrument information (technical characteristics, reports, configuration control documents, drawings, public communications, etc.), to software development/control (including the tracking of each bit produced by each pipeline). For this purpose, an Integrated Data and Information System (IDIS) was developed. IDIS (Bennett et al. 2000) is a collection of infrastructure software for supporting the Planck Data Processing Centres in their management of large quantities of software, data and ancillary information. The infrastructure is relevant to the development, operational and post-operational phases of the mission.

The full IDIS can be broken down into five major components:

- DMS Document Management System - to store and share documents
- DMC Data Management Component, allowing the ingestion, efficient management and extraction of the data (or subsets thereof) produced by Planck activities.
- SWC Software Component, allowing to administer, document, handle and keep under configuration control the software developed within the Planck project.
- ProC Process Coordinator, allowing the creation/run of processing pipelines inside a predefined and well controlled environment.
- FL Federation Layer, allowing the access control to the previous object and that act as a glue between there.

The use of the DMS allowed the entire consortia to store hundreds of document with an efficient way to retrieve them. The DMC is one API (application programming interface) for the data input/output versus a database (relational or object oriented) for the archiving of the data itself and its meta-information and it is provided with a user GUI. The ProC is a controlled environment in which each software module can be add to create an entire functional pipeline, it store all the information regarding versioning of the modules used, data, temporary data created in the database using the DMC API. In Fig 16 an example of LFI pipeline is shown. And finally the FL is an API that using a remote LDAP database, assign the right permission to the users respect data access, software access and pipeline run.

### 6.6. DPC Test performed

Each pipeline and sub-pipeline (Level 1, Level 2 and Level 3) were subject to different kind of tests. We report here only the so-called “official tests” without referring to the internal tests that are more module-oriented.

The Level 1 was the most heavily tested as this pipeline is considered launch-critical. As a first step it was necessary to validate the output with respect to the input: to do that we ingested in the instrument a well known signal as described in (Frailis et al. 2009) with the purpose of verifying if the processing inside Level 1 was correct. Afterwards more complete tests, including all interfaces with other elements of the ground segment, were performed. Those tests simulate one week of nominal operations (SOVT1 - System Operation Validation Test) (Keck 2008) and, during the SOVT2, one week of Commissioning Performance Verification (CPV) phase. During this test we demonstrated that the LFI Level 1 is able to deal with the telemetry as it should be acquired during operations.

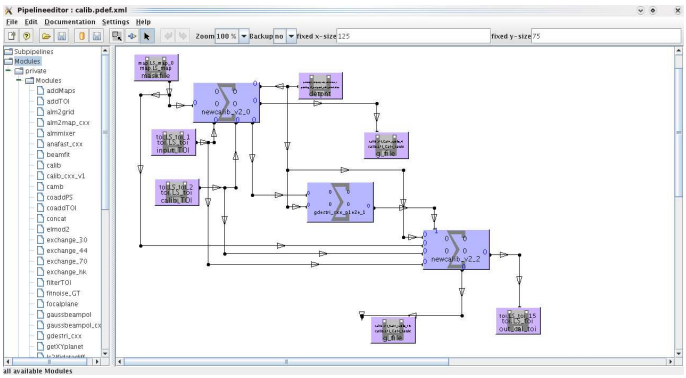

**Figure 16.** IDIS ProC pipeline Editor.

Tests performed on Level 2 and Level 3 were more science oriented to demonstrate the scientific adequacy of the LFI DPC pipeline, i.e. its ability to produce scientific results commensurate to the objectives of the Planck mission. These test were based on blind simulation of growing complexity. The test Phase 1, produced with the Level S, assumed some simplifying approximations:

- the sky model was based on the “convergence model” CMB (no non-gaussianity);
- the dipole did not include modulations due to Lissajous orbit around L2;
- Galactic emission was obtained assuming non-spatially varying index;
- the detector model was “ideal” and did not vary with time;
- the scanning strategy was “ideal” (i.e. no gaps in the data).

and the results were in line with the objective of the mission, see (Perrotta & Maino 2007).

The test phase 2 is still ongoing. It takes into account more realistic simulations with all the known systematics and known problems (e.g. data gaps) in the data. Results are expected in May 2009.

## 7. Conclusion

LFI works as expected. The programme starts on May 14th.

A challenging commissioning and final calibration phase will prepare the LFI for nominal operations that will start about 90 days after launch. After ~20 days the instrument will be switched on and its functionality will be tested in parallel with the cooldown of the 20 K stage. Then the cooldown of the HFI focal plane down to 4 K will be exploited by the LFI to tune voltage biases of the front end amplifiers and phase switches, which will set the instrument final scientific performances. Last tunings and calibration will be performed in parallel with HFI activities for about 25 days until the last in-flight calibration phase (the so-called “first light survey”), 14 days of data acquisition in nom-

inal mode that will benchmark the whole system, from satellite and instruments to data transmission, ground segment and data processing levels.

The first light survey will produce the very first Planck maps. This will not be aimed to scientific exploitation but will rather serve as a final test of the instrumental and data processing capabilities of the mission. After this, the Planck scientific operations will begin.

## 8. Acknowledgements

Planck is a project of the European Space Agency with instruments funded by ESA member states, and with special contributions from Denmark and NASA (USA). The Planck-LFI project is developed by an International Consortium lead by Italy and involving Canada, Finland, Germany, Norway, Spain, Switzerland, UK, USA. The Italian contribution to Planck is supported by the Italian Space Agency (ASI). We wish also to thank people of the Herschel/Planck Project of ESA, ASI, THALES Alenia Space Industries, and the LFI Consortium that are involved in activities related to optical simulations.

## References

????
Abdo, A. A. 2009, ArXiv e-prints
Abramo, L. R., Bernui, A., Ferreira, I. S., Villela, T., & Wuensche, C. A. 2006, Phys. Rev. D, 74, 063506
Artal, E., Aja, B., L. de la Fuente, M., et al. 2009, A&A, this volume
Ashdown, M. A. J., Baccigalupi, C., Balbi, A., et al. 2007a, A&A, 471, 361
Ashdown, M. A. J., Baccigalupi, C., Balbi, A., et al. 2007b, A&A, 467, 761
Ashdown, M. A. J., Baccigalupi, C., Balbi, A., et al. 2007c, A&A, 467, 761
Bartolo, N., Komatsu, E., Matarrese, S., & Riotto, A. 2004, Phys. Rep., 402, 103
Bartolo, N. & Riotto, A. 2009, Journal of Cosmology and Astro-Particle Physics, 3, 17
Bennett, K., Pasian, F., Sygnet, J.-F., et al. 2000, in Society of Photo-Optical Instrumentation Engineers (SPIE) Conference Series, Vol. 4011, Society of Photo-Optical Instrumentation Engineers (SPIE) Conference Series, ed. R. I. Kibrick & A. Wallander, 2–10
Bersanelli, M., Mattaini, E., Santambrogio, E., et al. 1998, Experimental Astronomy, 8, 231
Burigana, C., Malaspina, M., Mandolesi, N., et al. 1999, ArXiv Astrophysics e-prints
Burigana, C., Natoli, P., Vittorio, N., Mandolesi, N., & Bersanelli, M. 2001, Experimental Astronomy, 12
Chu, M., Eriksen, H. K., Knox, L., et al. 2005, Phys. Rev. D, 71, 103002
Collaudin, B. & Passvogel, T. 1999, Cryogenics, 39, 157
Copi, C. J., Huterer, D., Schwarz, D. J., & Starkman, G. D. 2007, Phys. Rev. D, 75, 023507
Copi, C. J., Huterer, D., Schwarz, D. J., & Starkman, G. D. 2008, ArXiv e-prints
Copi, C. J., Huterer, D., & Starkman, G. D. 2004, Phys. Rev. D, 70, 043515
Cuttaia, F., Bersanelli, M., Battaglia, P., et al. 2009, A&A, this volume
D'Arcangelo, O., Figini, L., Simonetto, A., et al. 2009, A&A, this volume
Davis, R., Wilkinson, A., Davies, R., et al. 2009, A&A, this volume
de Gasperis, G., Balbi, A., Cabella, P., Natoli, P., & Vittorio, N. 2005, A&A, 436, 1159
Dunkley, J., Komatsu, E., Nolta, M. R., et al. 2009, ApJS, 180, 306
Dupac, X. & Tauber, J. 2005, A&A, 430, 363
Eriksen, H. K., Hansen, F. K., Banday, A. J., Górski, K. M., & Lilje, P. B. 2004a, ApJ, 605, 14
Eriksen, H. K., Hansen, F. K., Banday, A. J., Górski, K. M., & Lilje, P. B. 2004b, ApJ, 609, 1198
Fermi/LAT Collaboration: W. B. Atwood. 2009, ArXiv e-prints
Frailis, M., Maris, M., Zacchei, A., et al. 2009, A&A, this volume
Gentili, G., Nesti, R., Peolsi, G., & Natale, V. 2000, Electr. Lett., 36, 486
Hamimeche, S. & Lewis, A. 2008, Phys. Rev. D, 77, 103013
Hinshaw, G., Banday, A. J., Bennett, C. L., et al. 1996, ApJ, 464, L17+
Holman, R. & Tolley, A. J. 2008, Journal of Cosmology and Astro-Particle Physics, 5, 1
Keck, F. 2008, Planck SOVT1 Test Report, Tech. Rep. PT-PMOC-OPS-RP-6414-OPS-OAP, ESOC Documentation
Komatsu, E., Dunkley, J., Nolta, M. R., et al. 2009, ApJS, 180, 330
Land, K. & Magueijo, J. 2005, Physical Review Letters, 95, 071301
Maino, D., Burigana, C., Maltoni, M., et al. 1999a, A&AS, 140, 383
Maino, D., Burigana, C., Maltoni, M., et al. 1999b, A&AS, 140, 383
Mandolesi, N., Bersanelli, M., Burigana, C., et al. ????
Maris, M., Bersanelli, M., Burigana, C., et al. 2006, Memorie della Societa Astronomica Italiana Supplement, 9, 460
Mennella, A., Bersanelli, M., Aja, B., et al. 2009, A&A, this volume
Mennella, A., Bersanelli, M., Burigana, C., et al. 2002, A&A, 384, 736
Morgante, G. 2009a, A&A, this volume
Morgante, G., P. D. S. P. T. L. e. a. 2009b, A&A, this volume
Natoli, P., de Gasperis, G., Gheller, C., & Vittorio, N. 2001, A&A, 372, 346
Pasian, F., Bersanelli, M., & Mandolesi, N. 2000, Baltic Astronomy, 9, 511
Pasian, F. & Gispert, R. 2000, Astrophysical Letters Communications, 37, 247
Pasian, F. & Sygnet, J.-F. 2002, in Society of Photo-Optical Instrumentation Engineers (SPIE) Conference Series, Vol. 4847, Society of Photo-Optical Instrumentation Engineers (SPIE) Conference Series, ed. J.-L. Starck & F. D. Murtagh, 25–34
Perrotta, F. & Maino, D. 2007, Planck LFI - SGS2 End-to-End test report, Tech. Rep. PL-LFI-OAT-RP-010, LFI DPC Documentation
Poutanen, T., de Gasperis, G., Hivon, E., et al. 2006, A&A, 449, 1311
Reinecke, M., Dolag, K., Hell, R., Bartelmann, M., & Enßlin, T. A. 2006, A&A, 445, 373
Schwarz, D. J., Starkman, G. D., Huterer, D., & Copi, C. J. 2004, Physical Review Letters, 93, 221301
Smith, K. M., Senatore, L., & Zaldarriaga, M. 2009a, ArXiv e-prints
Smith, K. M., Senatore, L., & Zaldarriaga, M. 2009b, ArXiv e-prints
Smith, K. M. & Zaldarriaga, M. 2006, ArXiv Astrophysics e-prints
Smoot, G. F., Bennett, C. L., Kogut, A., et al. 1992a, ApJ, 396, L1
Smoot, G. F., Bennett, C. L., Kogut, A., et al. 1992b, ApJ, 396, L1
Tegmark, M. 1997, ApJ, 480, L87+
Tegmark, M., de Oliveira-Costa, A., & Hamilton, A. J. 2003, Phys. Rev. D, 68, 123523
Terenzi, L., Bersanelli, M., Battaglia, P., et al. 2009a, A&A, this volume
Terenzi, L., Bersanelli, M., Mennella, A., et al. 2009b, A&A, this volume
Valenziano, L., V. F. M. N. & Bersanelli, M. ????, Focal Surface Evaluation for the Planck Telescope, Tech. rep., TESRE/CNR - Bologna
Varis, J., Hughes, N., Laaninen, M., et al. 2009, A&A, this volume
Vielva, P., Martínez-González, E., Barreiro, R. B., Sanz, J. L., & Cayón, L. 2004, ApJ, 609, 22
Villa, F., Bersanelli, M., Cappellini, B., et al. 2009a, A&A, this volume
Villa, F., D'Arcangelo, O., Pagana, E., et al. 2009b, A&A, this volume
Villa, F., D'Arcangelo, O., Pecora, M., et al. 2009c, A&A, this volume
Villa, F., Sandri, M., Mandolesi, N., et al. 2002, Experimental Astronomy, 14, 1
Weeks, J. R. 2004, ArXiv Astrophysics e-prints
Yadav, A. P. S., Komatsu, E., & Wandelt, B. D. 2007, ApJ, 664, 680
Zacchei, A., Frailis, M., Maris, M., et al. 2009, A&A, this volume